Polarization 101 Exercise:
- build a “polarization application” statement for your research -

SHUG 2023, Polarization Town Hall

Polarized neutrons enable a variety of capabilities which enhance ‘unpolarized’ neutron scattering techniques by separating different aspects and dimensions of scattering, or by providing high-resolution in energy and/or angle. This poster / handout is intended for prospective users of polarized neutrons, as a workflow to determine whether and how polarized neutrons might help you answer some of your more pressing questions, to navigate the wide range of capabilities, and to help you prepare proposals for experiments. This template approach is utilized in neighboring posters / handouts to provide a consistent framework for understanding the wide range of applications which leverage polarized neutrons, and to clarify which neutron scattering instruments can access which configurations.

STATEMENT TEMPLATE

As a [***SCIENCE AREA***] neutron scattering experimentalist, I want to [***CAPABILITY FAMILY***] when using [***NEUTRON SCATTERING TECHNIQUE***] with [***NEUTRON POLARIZATION CONFIGURATION***] so I can [***APPLICATION statement***] for [***SCIENCE EXAMPLE***]

SCIENCE AREA

- Biology
- Soft matter & Polymers
- Materials & Engineering
- Condensed matter & Quantum materials
- Chemistry / Geology
- Environmental Science

SCIENCE EXAMPLE

- What system(s) or material(s) are you studying right now?

NEUTRON SCATTERING TECHNIQUE

Structure
- Imaging
- Reflectometry
- (μ)Small Angle Neutron Scattering
- Diffraction (powder or single crystal)

Dynamics
- Quasielastic Scattering
- Direct Geometry / Triple Axis Spectroscopy
- Indirect Geometry Spectroscopy

UNPOLARIZED LIMITATION?

- …with the unpolarized data you’ve already obtained and are trying to analyze.
- Do you need to separate contributions to the observed scattering?
- Do you need enhanced momentum and / or energy resolution?

CAPABILITY FAMILY

Isolate nuclear scattering	N & I_N
Isolate spin-incoherent scattering	I_{si}
Leverage dynamic nuclear polarization	$N \leftrightarrow I_{si}$
Solve Phase Problem	N & $\boldsymbol{M}_\perp$
Explore magnetic scattering	$\boldsymbol{M}_\perp$
Explore coinciding of nuclear and magnetic scattering	N with $\boldsymbol{M}_\perp$
Explore magnetic chirality	$\boldsymbol{M}_\perp$ cross terms
Enhance time / energy resolution	I_N, I_{si}, N & $\boldsymbol{M}_\perp$
Enhance Q / size resolution	N & $\boldsymbol{M}_\perp$
Match resolution to dispersion	N & $\boldsymbol{M}_\perp$

APPLICATION STATEMENT

- Describe how this capability family will remove the unpolarized limitation and help you better understand your science example

$N(\boldsymbol{Q}) = \sum_n b_n e^{i\boldsymbol{Q}\cdot\boldsymbol{R}_n}$	Nuclear structure factor
$\boldsymbol{M}_\perp = \boldsymbol{e}_{\boldsymbol{Q}} \times \boldsymbol{M}(\boldsymbol{Q}) \times \boldsymbol{e}_{\boldsymbol{Q}}$	“M perpendicular”
$\boldsymbol{M}(\boldsymbol{Q}) = \sum_n \boldsymbol{M}_n e^{i\boldsymbol{Q}\cdot\boldsymbol{R}_n}$	Fourier transform of magnetic moments / magnetic structure factor
$\boldsymbol{e}_{\boldsymbol{Q}} = \boldsymbol{Q}/\lvert\boldsymbol{Q}\rvert$	Unit vector along momentum transfer **Q**
I_{si}	Spin incoherent scattered intensity
$\boldsymbol{P}, \boldsymbol{P}^1$	Initial and final polarization

MALEEV-BLUME EQUATIONS ACCESS SCATTERED INTENSITY & CHANGES IN NEUTRON POLARIZATION STATE

$$I = N^\dagger N + I_{si} + \boldsymbol{M}_\perp^\dagger \boldsymbol{M}_\perp + \boldsymbol{P}\cdot\boldsymbol{M}_\perp^\dagger N + \boldsymbol{P}\cdot\boldsymbol{M}_\perp N^\dagger + i\boldsymbol{P}\cdot\left(\boldsymbol{M}_\perp^\dagger \times \boldsymbol{M}_\perp\right)$$

$$\boldsymbol{P}^1 I = \boldsymbol{P}\left(I_n + N^\dagger N - \frac{1}{3} I_{si}\right) + \left(\boldsymbol{P}\cdot\boldsymbol{M}_\perp^\dagger\right)\boldsymbol{M}_\perp + \left(\boldsymbol{P}\cdot\boldsymbol{M}_\perp\right)\boldsymbol{M}_\perp^\dagger - \boldsymbol{P}\left(\boldsymbol{M}_\perp^\dagger \boldsymbol{M}_\perp\right) + iN\left(\boldsymbol{P}\times\boldsymbol{M}_\perp^\dagger\right) - iN^\dagger\left(\boldsymbol{P}\times\boldsymbol{M}_\perp\right) + N\boldsymbol{M}_\perp^\dagger + N^\dagger\boldsymbol{M}_\perp - i\left(\boldsymbol{M}_\perp^\dagger\times\boldsymbol{M}_\perp\right)$$

SEPARATE: IDENTIFY RELEVANT TERMS IN M-B EQUATIONS…

- Applications which separate or isolate (spin) incoherent from coherent, or magnetic direction-dependent contributions
- Select one or a few terms in the Maleev-Blume equations which speak to the capability which you intend to leverage
- **Special case #1:** Coalign system nuclei to switch from I_{si} to N
- **Special case #2:** two different $\boldsymbol{M}_\perp$ substrates to solve phase problem
- **Special case #3:** $\boldsymbol{P} \parallel \boldsymbol{P}^1$, *i.e.* change in polarization state is other than just ‘spin flip’ or ‘non-spin-flip’ due to cross terms (chirality and lattice-magnetic interference)

RESOLUTION: IDENTIFY NEEDED ENHANCEMENT

- Applications which enhance resolution (energy, momentum transfer, or some combination) for a given neutron scattering technique (preserves the energy or momentum transfer range)
- **Special case #4:** Evaluation of polarization state is tied to deliberate precession / phasing of neutron polarization state. This manipulation of $\boldsymbol{P}$ & $\boldsymbol{P}^1$ *is not found* in the *M-B* equations
- Larmor precession: $\vec{\tau} = \vec{\mu} \times \vec{B},\ \omega = -\gamma B$

TO DETERMINE CONFIGURATION

POLARIZATION CONFIGURATION	Measures the scattered neutron	Optics
Half Polarized Dynamic Nuclear Polarization Solve Phase Problem	Intensity	1 filter 1 flipper
Longitudinal Analysis I Larmor	Polarization State	2 filters 1 flipper
Longitudinal Analysis II Spherical Neutron Polarimetry	Both	2 filters 2 flippers

- Fortunately, most terms in the *M-B* equations can be safely ignored by accounting for the physics of the system under study
- Becomes a linear / vector algebra problem, with multiple choices for incident ($\boldsymbol{P}$) and sometimes final ($\boldsymbol{P}^1$) polarization
- Polarization terminology for different scattering technique / instrument classes has developed independently, so this terminology is not universal

[1]S. V. **Maleev,** V. G. Bar'yaktar, and R. A. Suris, The scattering of slow neutrons by complex magnetic structures Sov. Phys. Solid State 4, 2533 (1963)
[2]M. **Blume**, Polarization effects in the magnetic elastic scattering of slow neutrons, Phys. Rev. 130, 1670 (1963).

Oak Ridge National Laboratory is managed by UT-Battelle LLC for the US Department of Energy

Neutron Polarization Optics & Competencies

Polarization Steering Committee & Neutron Optics & Polarization Group, SHUG 2023

J. Leiner, B. Winn

FILTERS & SPLITTERS

Polarization filters select those neutrons with one of two quantum polarization states, with respect to an ambient magnetic field, via transmission, reflection or diffraction. Polarization splitters reflect neutrons of one polarization state while transmitting the other. Different filters utilize different physics, are optimal in different neutron wavelength or energy ranges, have different angular acceptances, transmission, and degrees of polarization, and may or may not be compatible with strong stray magnetic fields.

HEUSLER CRYSTALS

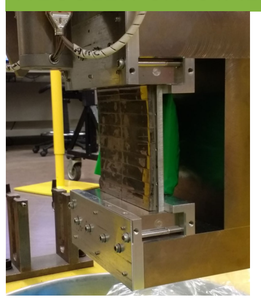

Magnetically saturated Heusler (Cu_2MnAl) crystals have a (111) Bragg peak which has nearly complete constructive (destructive) interference between nuclear and magnetic scattering lengths, depending on neutron spin state. This optic can then double as a diffraction crystal and as a polarization filter simultaneously.

At ORNL we utilize single crystals grown at ILL (a skill no longer available). ORNL provides crystal characterization and yoked assemblies, and shares several stand-alone standards for polarization characterization between instruments. Heusler arrays are used at PTAX and HYSPEC.

SUPERMIRROR ARRAYS

ORNL owns several arrays, some dedicated to specific instruments & others shared (available via the NOP Group). The NOP group helps instrument teams prepare specifications for mirror purchases.

SINGLE MIRROR

CURVED BENDERS

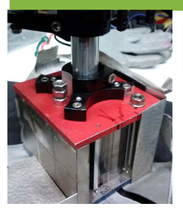

WIDE-ANGLE ARRAY

A 60°x15° wide angle array was developed and constructed by the Paul-Sherrer Institut for HYSPEC

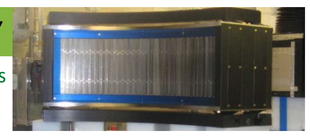

S-BENDERS

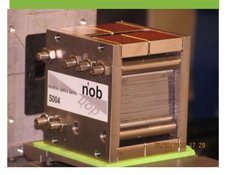

FAN ANALYZER

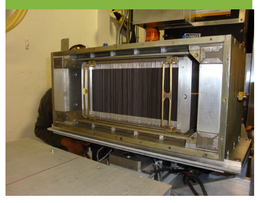

V-CHANNEL

^{3}He FILTER

These filters co-align the nuclei of ^{3}He atoms. Those neutrons with spin anti-parallel to the ^{3}He nuclei spin are preferentially absorbed. High field uniformity and special glass surfaces are required to minimize ^{3}He depolarization. The NOP group provides operational support for drop-in cells, and in-situ systems, in active development for a decade, provide stable, low maintenance performance.

SPIN-EXCHANGE OPTICAL PUMPING (SEOP) CHARGING STATIONS

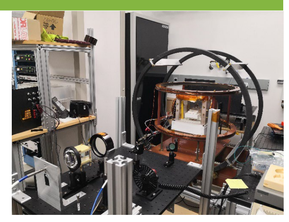

DROP IN

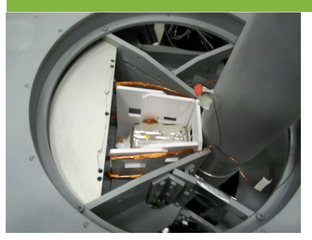

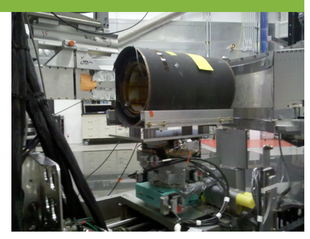

IN-SITU

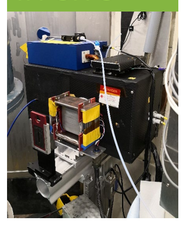

LOW ABBERRATION COILS

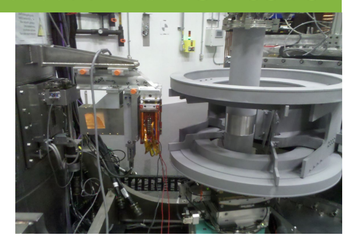

POLARIZATION DEVELOPMENT STATIONS @ HFIR

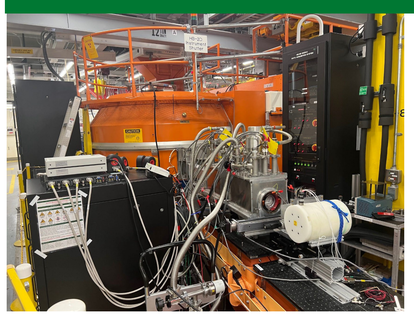

GUIDE FIELDS & NUTATORS

Guide fields provide ambient magnetic field (10-50 Gauss) in the neutron flight path, parallel or anti-parallel to the neutron moment, in which the neutron experiences Larmor precession. If the precession frequency is fast with respect to changes in the guide field direction, the neutrons 'nutate' or remain aligned with the changing guide field.

YOKED /w PM

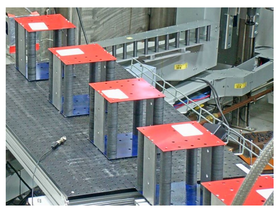

3D COILS

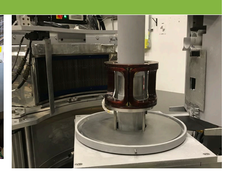

NUTATORS

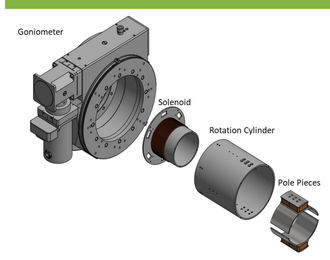

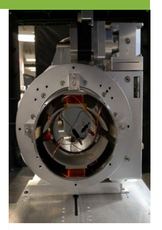

DEVELOPMENT LABS @ SNS

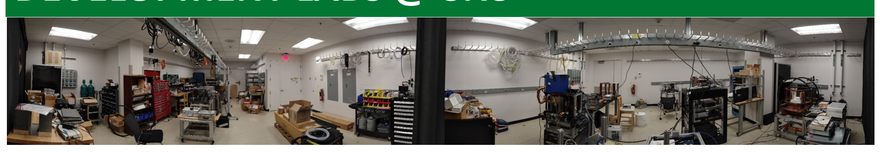

FLIPPERS

Flippers change the neutron polarization with respect to the ambient guide field, between parallel and anti-parallel. Some flippers can in principle establish other neutron polarization directions but when using a guide field this depolarizes the beam.

MEZEI

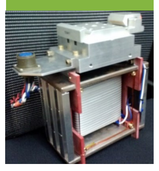

RF

CRYO

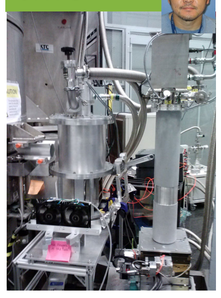

^{3}He FILTER ADIABATIC FAST PASSAGE

ZERO-FIELD CHAMBERS & PRECESSION CHAMBERS

Zero-field chambers are required for the Spherical Neutron Polarimetry configuration, useful for measuring off-diagonal elements of the polarization tensor. They are also useful for studying materials in the superconducting state with polarized neutrons, since they establish a separate and well-defined Meissner screen geometry. Precession chambers utilize superconducting coils and Meissner screens to achieve conditions analogous to the 'compensation' coil of Mezei flippers, and enable neutron orientations not parallel to the precession chamber surfaces. At ORNL, we utilize a combination of μ-metal (room temperature or below), YBCO film on flat substrates (20 K with 1st stage CCR), and/or Niobium foil (<8 K with 2nd stage CCR) to achieve these conditions. The SNP system is already available via the user program for PTAX, and will be at GP-SANS once polarization filters are implemented in a planned upgrade. Wide-angle SNP is a configuration undergoing active development and design.

μ-METAL

CRYOSTATS

PRECESSION CHAMBER /W YBCO MEISSNER SCREENS

LARMOR COMPONENTS

Larmor components enable Larmor labeling or encoding, for enhanced sensitivity to a neutrons speed or direction. In contrast to guide fields and nutators, Neutron Spin Echo (NSE) coils and Wollaston prisms establish a magnetic field perpendicular to the neutron polarization. The Mezei flipper or precession chamber concepts can be modified to create a π/2 rotation from guide field to precession field.

NSE COILS

CRYOSTATS

YBCO WOLLASTON PRISM

FAST DETECTORS

SUPERCONDUCTING RF FLIPPERS

DYNAMIC NUCLEAR POLARIZATION

SYSTEM TO POLARIZE HYDROGEN NUCLEI

SOFTWARE

MODELING & DESIGN

The NOP Group utilizes both MAGNET® and COMSOL®[2] for 3D magnetic modeling, and McStas[1] for polarized neutron optics design.

EXPERIMENT PLANNING

A variety of planning tools have been developed for various kinds of experiments.

ACQUISITION

Acquisition[2] leverages EPICS at the SNS and (for now) SpICE at HFIR.

DATA REDUCTION & ANALYSIS

Reduction software has (to some extent) been integrated with the MANTID python package.

Research was performed at HFIR and SNS, DOE Office of Science User Facilities

[1]Willendrup, P.K., Lefmann, K., "McStas (ii): An overview of components, their use, and advice for user contributions" *J. of Neutron Research* **23** 7 (2021)
[2]Silva, N., "Wide-Angle Spherical Neutron Polarimetry at Oak Ridge National Laboratory," dissertation, University of Florida (2023)

OAK RIDGE National Laboratory | HIGH FLUX ISOTOPE REACTOR | SPALLATION NEUTRON SOURCE

Oak Ridge National Laboratory is managed by UT-Battelle LLC for the US Department of Energy

U.S. DEPARTMENT OF ENERGY | Office of Science

Half Polarized Configuration
(1 filter, 1 flipper, scattered intensity variations only)
Powder & Single Crystal Diffraction

SHUG 2023, Polarization Town Hall

The Half-Polarized Configuration is readily accessible at several instruments via the user program.
Exciting new contrast-enhancing Capabilities and Applications are on the horizon.

MALEEV-BLUME EQUATION FOR SCATTERED INTENSITY

$$I = N^{\dagger}N + I_{si} + \boldsymbol{M}_{\perp}^{\dagger}\boldsymbol{M}_{\perp} + \boldsymbol{P}\cdot\boldsymbol{M}_{\perp}^{\dagger}N + \boldsymbol{P}\cdot\boldsymbol{M}_{\perp}N^{\dagger} + i\boldsymbol{P}\cdot\left(\boldsymbol{M}_{\perp}^{\dagger}\times\boldsymbol{M}_{\perp}\right)$$

With both polarized neutrons and polarized nuclei, one can shift scattered intensity from spin incoherent scattering to nuclear coherent scattering (and we're hiding a $\boldsymbol{P}$)

Independent of polarization state so not directly used for half polarized work

Magnetization density and local site magnetic susceptibility in paramagnets, ferrimagnets and ferromagnets, and Interference of magnetic and nuclear scattering

Chiral magnetic structures in antiferromagnets

$N(\boldsymbol{Q}) = \sum_n b_n e^{i\boldsymbol{Q}\cdot\boldsymbol{R}_n}$	Nuclear structure factor
$\boldsymbol{M}_{\perp} = \boldsymbol{e}_{\boldsymbol{Q}} \times \boldsymbol{M}(\boldsymbol{Q}) \times \boldsymbol{e}_{\boldsymbol{Q}}$	"M perpendicular"
$\boldsymbol{M}(\boldsymbol{Q}) = \sum_n \boldsymbol{M}_n e^{i\boldsymbol{Q}\cdot\boldsymbol{R}_n}$	Fourier transform of magnetic moments / magnetic structure factor
$\boldsymbol{e}_{\boldsymbol{Q}} = \boldsymbol{Q}/\lvert\boldsymbol{Q}\rvert$	Unit vector along momentum transfer **Q**
I_{si}	Spin incoherent scattered intensity
$\boldsymbol{P}, \boldsymbol{P}^1$	Initial and final polarization

PTAX (HB-1, HFIR)

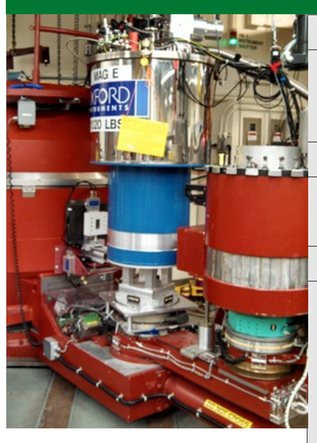

Science Area	Condensed matter
Science Example	MnP single crystal, helical magnet which exhibits superconductivity under high pressure
Capability Family	Explore magnetic chirality
Relevant M-B terms	$i\boldsymbol{P}\cdot\left(\boldsymbol{M}_{\perp}^{\dagger}\times\boldsymbol{M}_{\perp}\right)$
Capability	Chirality
Application Statement	By aligning the neutron spin parallel and antiparallel to h, the magnetic intensities from two helical domains with clockwise and counter-clockwise helicities can be observed, respectively

M. Matsuda et al., *Physica B* **551** 115 (2018)

Sc. A.	Condensed matter
Sc. Ex.	EuPtSi single crystal, skyrmion material
Cap. Fam.	Explore magnetic chirality
M-B	$i\boldsymbol{P}\cdot\left(\boldsymbol{M}_{\perp}^{\dagger}\times\boldsymbol{M}_{\perp}\right)$
Cap.	Chirality
App. St.	Evaluate existence of chirality and its domain population

K. Kaneko et al., *J. Phys. Soc. Jpn.* **88** 013702 (2019)

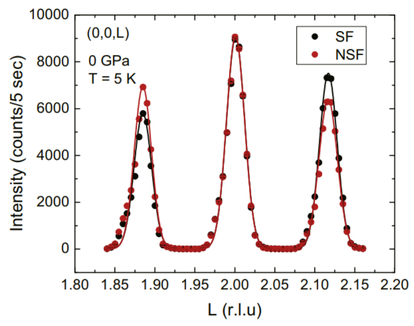

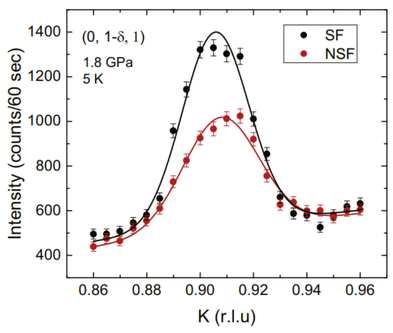

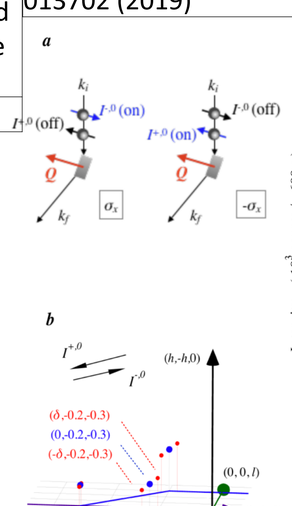

Neutron diffraction intensities in the NSF and SF channels around the (0, 0, 2 ±δ) magnetic Bragg reflections at 5 K and at ambient pressure (a) and the (0, 1 − δ, 1) magnetic Bragg reflection at 5 K and at 1.8 GPa (b)

(a) Schematic drawing of the half polarized scattering setup at HB-1. Neutron spin is polarized parallel=antiparallel to the scattering vector Q. Setup for was realized by reversing the sign of the guide field. (b) Illustrative scan trajectory and positions of magnetic peaks in the ground state (blue) and the intermediate phase (red) with respect to the horizontal ðh; h; lÞ scattering plane. (c)–(e) Incident polarization dependence of scans along ðh; h; 0Þ across ð0; 0:2; 0:3Þ measured at (c) 1.5 K, (d) 1.5 K with reversed guide field, and (e) 3.0 K with original guide field.

POWDER (HB-2A, HFIR)

Sc. A.	Condensed matter
Sc. Ex.	$M(N_2H_5)_2(SO_4)_2$ powder, metal-organic frameworks (MOF's) with 1D spin chains
Cap. Fam.	Explore magnetic scattering
M-B	$\boldsymbol{P}\cdot\boldsymbol{M}_{\perp}^{\dagger}N + \boldsymbol{P}\cdot\boldsymbol{M}_{\perp}N^{\dagger}$
Cap.	Determine magnetization density
App. St.	show different site magnetization for M=Cu^{2+}, Co^{2+}, or Mn^{2+}

S. Calder et al., *Phys. Rev. Mater.* **6** 124407 (2022)

(left)
Difference measurements of $I_+ - I_-$ for $Mn(N_2H_5)_2(SO_4)_2$ and $Co(N_2H_5)_2(SO_4)_2$, and refined fit using a site susceptibility model.
(right)
The magnetization ellipsoid representation of the local site susceptibility for the Mn & Co ion, respectively

Analysis performed with CrysPy
https://sites.google.com/view/cryspy

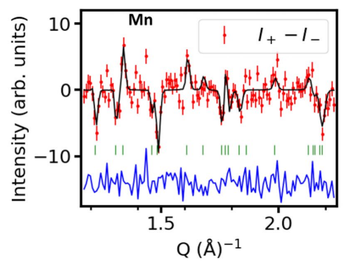

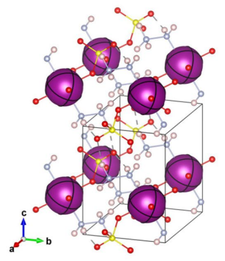

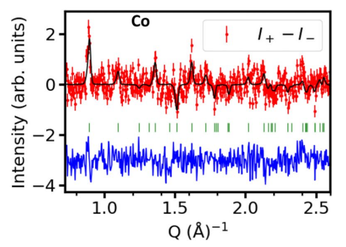

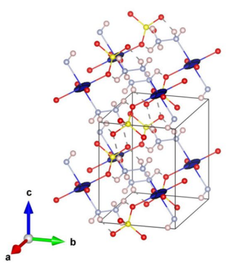

DEMAND (HB-3A, HFIR)

Sc. A.	Condensed matter
Sc. Ex.	$MnBi_4Te_7$ single crystal, a 2D van der Waals system and magnetic topological insulators rendering quantum anomalous Hall effect and diverse topological states
Cap. Fam.	Explore magnetic scattering
M-B	$\boldsymbol{P}\cdot\boldsymbol{M}_{\perp}^{\dagger}N + \boldsymbol{P}\cdot\boldsymbol{M}_{\perp}N^{\dagger}$
Cap.	Determine magnetization density
App. St.	Flipping ratio of 136 reflections enables conversion to magnetization density

Lei Ding et al., *J. Phys. D: Appl. Phys.* **54** 74003 (2021)

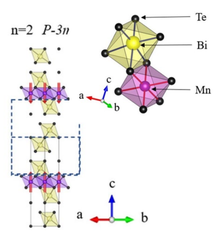

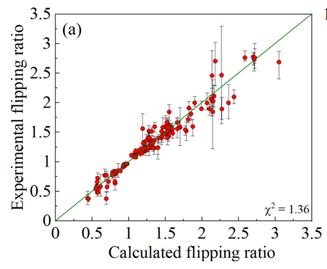

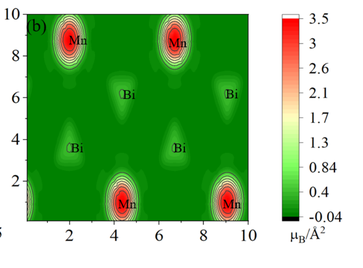

(a) The observed and calculated flipping ratios using 136 reflections. (b) Projection of the spin density within the unit cell on the (ab)-plane for $MnBi_4Te_7$ under the magnetic field of 0.83 T.

IMAGINE (CG-4D, HFIR)

Sc. A.	Biology
Sc. Ex.	wt*T4L single crystal
Cap. Fam.	Dynamic Nuclear Polarization
M-B	$N^{\dagger}N + I_{si}$
Cap.	Dynamic Nuclear Polarization
App. St.	

J.Pierce et al, *in preparation*

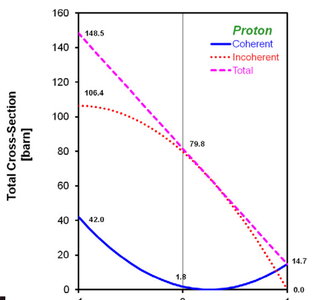

Anti-aligned - Aligned

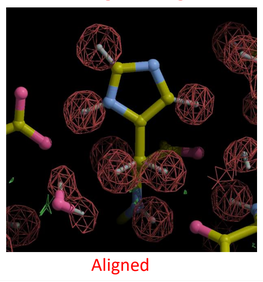

Aligned

Anti-aligned

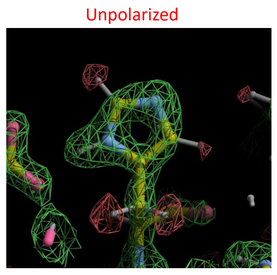

Unpolarized

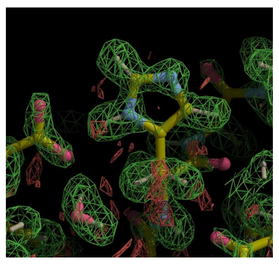

Aligned

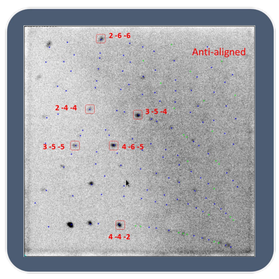

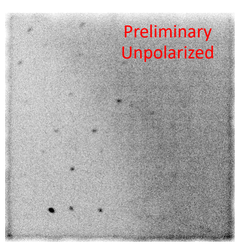

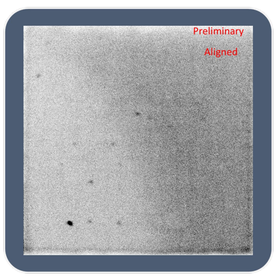

HYSPEC (BL-14B, SNS)

Sc. A.	Condensed matter
Sc. Ex.	$La_{0.4}Ce_{0.6}Co_2P_2$ powder, a weak ferromagnet which vanishes at a structural transition
Cap. Fam.	Explore magnetic scattering
M-B	$\boldsymbol{P}\cdot\boldsymbol{M}_{\perp}^{\dagger}N + \boldsymbol{P}\cdot\boldsymbol{M}_{\perp}N^{\dagger}$
Cap.	Determine Magnetization Density
App. St.	Measure weak 0.15(1) μ_B per Co atom

J.K. Clark et al, *Phys. Rev. Mat.* **4** 074412 (2020)

$\overrightarrow{\boldsymbol{H}} \,//\, \overrightarrow{\boldsymbol{P}} \,//\, \mathbf{z}$ (~ 0.5 T)

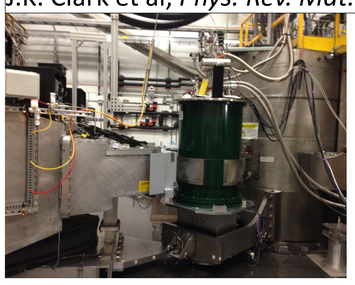

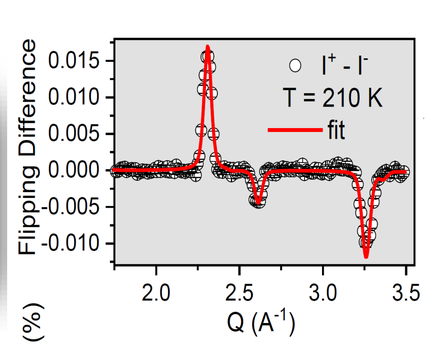

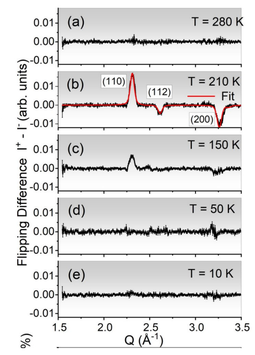

$La_{0.4}Ce_{0.6}Co_2P_2$ undergoes a weak ferromagnetic ordering at ~225 K (~0.15 mB per Co atom) followed by a structural collapse at ~190 K, which leads to a strong suppression of magnetization. A combination of magnetic measurements and polarized neutron scattering experiments suggests that $La_{0.4}Ce_{0.6}Co_2P_2$ enters a disordered state with gradual dissipation of the ferromagnetic ordering taking place simultaneously with the structural collapse.

[1]S. V. **Maleev,** V. G. Bar'yaktar, and R. A. Suris, The scattering of slow neutrons by complex magnetic structures Sov. Phys. Solid State 4, 2533 (1963)
[2]M. **Blume**, Polarization effects in the magnetic elastic scattering of slow neutrons, Phys. Rev. 130, 1670 (1963).

Oak Ridge National Laboratory is managed by UT-Battelle LLC for the US Department of Energy

Accelerating Discovery Using DNP-Enhanced Neutron Protein Crystallography

Neutron Scattering Division: Josh Pierce, Malcolm Cochran, Flora Meilleur, Andrey Kovalevsky, Zach Morgan, Bryan Chakoumakos, Dean Myles

Neutron Technologies Division: Dominic Giuliano, Matt Loyd, Lowell Crow, Matt Frost, Amy Jones

Spin Dependence of Neutron Scattering from Hydrogen

- The spin dependence of the hydrogen cross section is large
  - For hydrogen $b = -3.74 + 14.56 \times P_n \times P_H$
- Nuclear incoherent scattering can be removed entirely (true for any nucleus)
- Coherent scattering can be increased by a factor of 7 (or 20)
- An increase in signal to noise enters **squared** in figure of merit
  - Factor of 10 in signal to noise is a factor of 100 in flux/sample size/data collection time
- The hydrogen nucleus is polarizable via Dynamic Nuclear Polarization, DNP

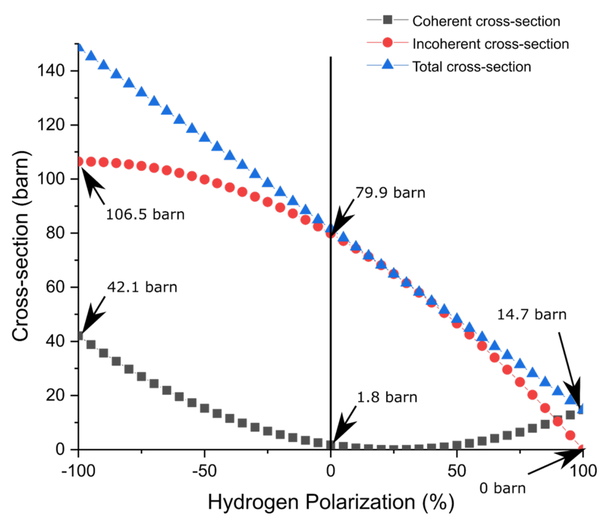

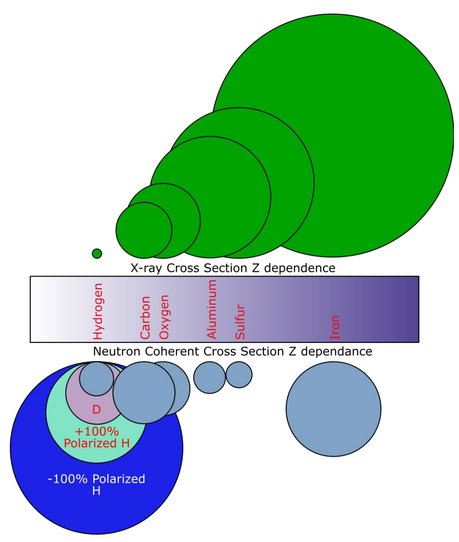

Breakthrough High Impact Biological Science

DNP-enhanced macromolecular crystallography will deliver >10-100 fold gains in performance for neutron analysis of hydrogenous materials, enabling break-throughs in our understanding and control of complex biological systems

- Large >> 10-100 fold increases in S/N of the data
- Amplifying diffraction intensity and minimizing incoherent scattering background
  - Higher resolution data from radically smaller protein crystals (< 0.01 mm^3)
  - More rapid data collection (hours or days)
  - Enables the visibility of hydrogen atoms to be amplified and enhanced in situ
  - New ways to collect, analyze and amplify diffraction from biological systems
- General – ALL hydrogenated proteins from ANY biological system.

Enabled Science and Capability

- **Radically smaller crystals (<< 0.01 mm^3)**
- **Larger proteins/complexes**
- **Membrane proteins**

DNP: Amplifying/tuning Hydrogen

Maximizes signal:	**Gain**	**↑ x8**
Minimizes background:	**Gain**	**↓ x10**

IMAGINE X:

Maximizes signal:	**Gain**	**↑ x2**
Minimizes background:	**Gain**	**↓ x4**
Together, DNP-IMAGINE-X	**Gains:**	**↑↑x10's**

Proof-of-Principle: Amplifying Hydrogen in Biological Crystals

- **Prototype: x~3 gains S/N** *(already comparable to Deuteration)*
  - 100% negative polarization: -18.30 fm
  - 100 % positive polarization: +10.82 fm
  - Dramatically enhances scattering/visibility of hydrogen
- **Tunable Difference Measurements**
  - Adiabatic Fast Passage or neutron spin flipper can reverse polarization more quickly
  - Only thing that changes is the cross section for the nuclei, and that changes in a predictable manner

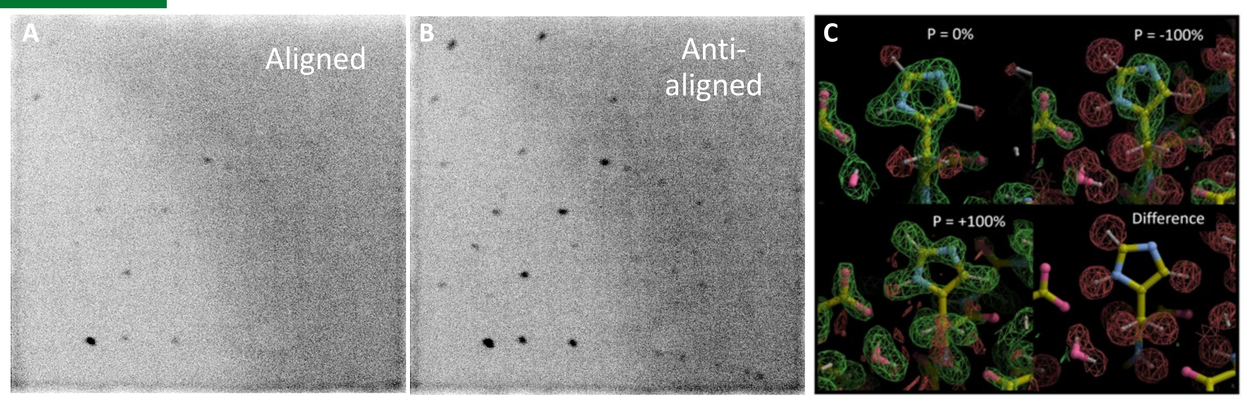

DNP NMC tunes the spin dependent scattering length of H_b by a near order of magnitude: A-B) Measured DNP NMC diffraction at ORNL: Spin aligned (A), Spin anti-aligned (B); C) Calculated DNP nuclear maps.

DNP-IMAGINE-X: unique capability and science

- **Continuous DNP system → 10-fold gains in S/N**
- Cryogen free, superconducting 5 T Helmholtz Coil
  - ~2π Acceptance for scattered neutrons
- High power, cryogen free 1 K recirculating ^{4}He refrigerator
- **SiPM based anger cameras → 5-fold gains in S/N**
  - 45 cm detector distance (like MaNDi)
  - 40 cameras in 2 banks (assuming current design)
- Tunable, reversible and in situ control (~10-fold) of spin-dependent coherent scattering within a single "perfectly isomorphous" sample
- (~100 mK), high field (5 T), cold (2-10 Å) neutron Laue diffraction experiments, well matched to advanced magnetic and quantum material science
- A new, unique capability that will open and extend new fields of neutron research and discovery for the decade(s) ahead

DNP-IMAGINE-X: conceptual design of the new DNP sample environment, detector banks and upstream neutron polarization and spin-flipper system, installed at the end station of the current IMAGINE beamline

Research was performed at the HFIR and SNS, DOE Office of Science User Facilities. Parts of the research were supported by ORNL's Laboratory Directed Research and Development (LDRD) program.

Longitudinal Polarized #1 Configuration

(2 filters, 1 flipper, spin-flip & non-spin-flip only)

Diffraction, Depolarization & Inelastic Scattering

SHUG 2023, Polarization Town Hall

M. Matsuda, O. Garlea, B. Winn

PTAX

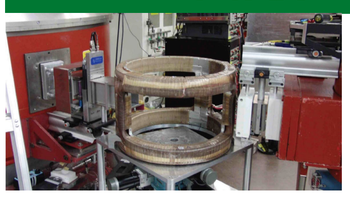

HYSPEC

Longitudinal-1 and 3D Polarization Analysis Configurations are readily accessible at these two spectrometers via the user program. Up to 8 T applied vertical field at both instruments is compatible with a 1D configuration, up to 0.8 T horizontal field via permanent magnet yoked systems is available, and for a wide range of temperatures a 3D configuration enables multi-dimensional access. HYSPEC's wide-angle supermirror array analyzer enables wide-angle polarization analysis. At both spectrometers, transition between polarized and unpolarized mid-experiment is routine.

DIFFRACTION

PTAX

Science Area	Condensed matter
Science Example	$PbCrO_3$ powder, a peroskovite with a charge-glass state
Capability Family	Isolate nuclear & magnetic scattering
Relevant M-B terms	$PN^{\dagger}N + (P\cdot M_{\perp}^{\dagger})M_{\perp} + (P\cdot M_{\perp})M_{\perp}^{\dagger} - P(M_{\perp}^{\dagger}M_{\perp})$
Capability	Isolate nuclear & magnetic scattering
Application Statement	Clarify nature of anomalous peak
R. Yu et al., *JACS* **137**, 12719 (2015)	

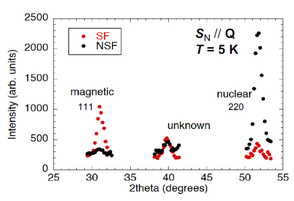

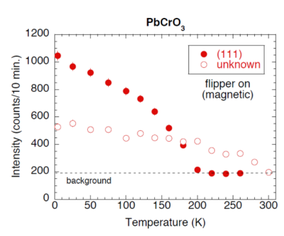

The 111 peak is magnetic in origin, but since the transition temperature is different from that of $PbCrO_3$, it should be attributed to the secondary phase, most probably to Pb_2CrO_5

Isolate nuclear coherent with isotope incoherent scattering

PTAX

Sc. A.	Condensed matter
Sc. Ex.	$Ba_3CoSb_2O_4$ single crystal, a spin-1/2 equilateral triangular-lattice antiferromagnet
Cap. Fam.	Explore magnetic scattering
M-B	$(P\cdot M_{\perp}^{\dagger})M_{\perp} + (P\cdot M_{\perp})M_{\perp}^{\dagger} - P(M_{\perp}^{\dagger}M_{\perp})$
Cap.	Determine spin directions
App. St.	Determine that the spins are in the ab plane
J. Ma et al., *Phys. Rev. Lett.* **116** 0872011 (2016)	

Isolate spin-incoherent scattering

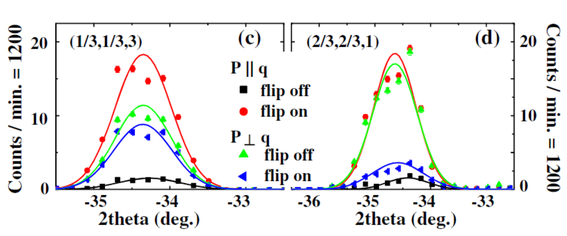

Index	I_{SF}/I_{NSF}	Magnetic model calculations: *ab* plane model	Magnetic model calculations: *ac* plane model
[2/3 2/3 1]	0.16(2)	0.12	0.88
[1/3 1/3 1]	0.36(3)	0.33	0.67
[1/3 1/3 3]	0.81(2)	0.82	0.18
[1/3 1/3 5]	0.94(2)	0.92	0.08

Separate contributions of different moments in the material to magnetic scattering

DEPOLARIZATION

HYSPEC

Sc. A.	Condensed matter
Sc. Ex.	$YbMnBi_2$ single crystal, a candidate Weyl metal
Cap. Fam.	Separate Mag. and Nuc. scattering
M-B	$PN^{\dagger}N + (P\cdot M_{\perp}^{\dagger})M_{\perp} + (P\cdot M_{\perp})M_{\perp}^{\dagger} - P(M_{\perp}^{\dagger}M_{\perp})$
Cap.	Separate magnetic and nuclear, and determine orientation of magnetic moment
App. St.	Confirm low temperature antiferromagnetic structure determined with unpolarized neutrons and refine Mn moment magnitude and direction
I. Zaliznyak et al, *J. Phys.: Conf. Ser.* **862** 012030 (2017)	

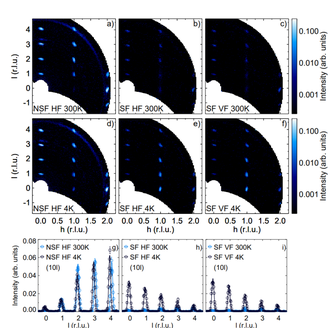

Sc. A.	Condensed matter
Sc. Ex.	$La_{0.4}Ce_{0.6}Co_2P_2$ powder, a weak magnet which vanishes at the structural transition
Cap. Fam.	Explore magnetic scattering
M-B	$(P\cdot M_{\perp}^{\dagger})M_{\perp} + (P\cdot M_{\perp})M_{\perp}^{\dagger} - P(M_{\perp}^{\dagger}M_{\perp})$
Cap.	Depolarization of transmitted beam
App. St.	Track magnetic order parameter as a function of temperature
J.K. Clark et al, *Phys. Rev. Mat.* **4** 074412 (2020)	

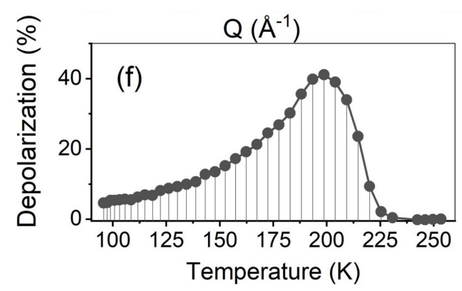

The temperature dependence of the neutron depolarization factor by the sample

MALEEV-BLUME EQUATION FOR SCATTERED NEUTRON POLARIZATION STATE

$$\boldsymbol{P}^{1}I = \boldsymbol{P}\left(I_n + N^{\dagger}N - \frac{1}{3}I_{si}\right) + (\boldsymbol{P}\cdot\boldsymbol{M}_{\perp}^{\dagger})\boldsymbol{M}_{\perp} + (\boldsymbol{P}\cdot\boldsymbol{M}_{\perp})\boldsymbol{M}_{\perp}^{\dagger} - \boldsymbol{P}(\boldsymbol{M}_{\perp}^{\dagger}\boldsymbol{M}_{\perp}) + iN(\boldsymbol{P}\times\boldsymbol{M}_{\perp}^{\dagger}) - iN^{\dagger}(\boldsymbol{P}\times\boldsymbol{M}_{\perp}) + N\boldsymbol{M}_{\perp}^{\dagger} + N^{\dagger}\boldsymbol{M}_{\perp} - i(\boldsymbol{M}_{\perp}^{\dagger}\times\boldsymbol{M}_{\perp})$$

Cannot explore either nuclear magnetic interference terms or chiral structures with only spin-flip and non-spin-flip operations at the sample. These are the only options because neutron spins can only be parallel or anti-parallel to the guide field.

INELASTIC SCATTERING

PTAX with magnet

Sc. A.	Condensed matter
Sc. Ex.	$Ba_2Mg_2Fe_{12}O_{22}$ single crystal, in field-induced noncollinear commensurate ferrimagnetic phase
Cap. Fam.	Explore magnetic scattering
M-B	$(P\cdot M_{\perp}^{\dagger})M_{\perp} + (P\cdot M_{\perp})M_{\perp}^{\dagger} - P(M_{\perp}^{\dagger}M_{\perp})$
Cap.	Determine orientation of mangetic excitations
App. St.	Determine that spin waves are transverse modes
T. Nakajima et al., *Phys. Rev. B* **93**, 035119 (2016)	

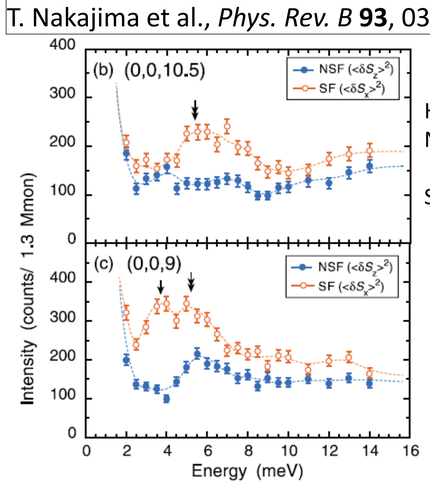

$\boldsymbol{S_N \perp Q}$

H = 1 T (FE3 phase)

Non-spin-flip (**NSF**): longitudinal

Spin-flip (**SF**): transverse

Isolate spin-incoherent scattering

HYSPEC

Sc. A.	Chemistry
Sc. Ex.	H_2O and D_2O
Cap. Fam.	Isolate spin-incoherent scattering
M-B	$PN^{\dagger}N - \frac{1}{3}PI_{si}$
Cap.	Separate nuclear scattering from spin-incoherent scattering
App. St.	Isolate autocorrelation function for both water and deuterated water
I. Zaliznyak et al, in preparation	

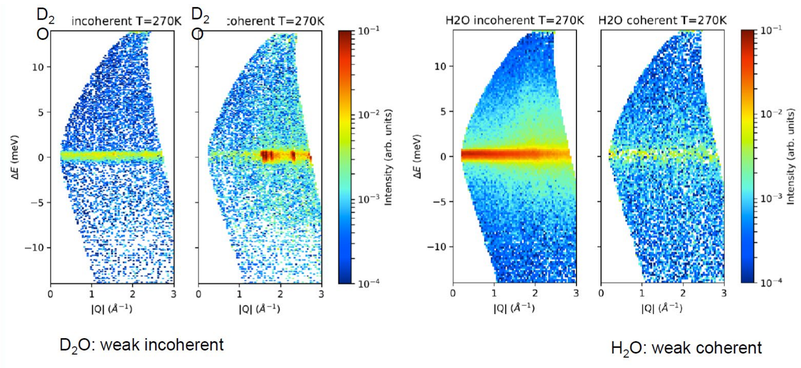

Separate contributions of different moments in the material to magnetic scattering

HYSPEC with magnet

Sc. A.	Condensed matter
Sc. Ex.	$Ba_2FeSi_2O_7$ single crystal, an S=1 antiferromagnet with strong easy-plane anisotropy
Cap. Fam.	Explore magnetic scattering
M-B	$(P\cdot M_{\perp}^{\dagger})M_{\perp} + (P\cdot M_{\perp})M_{\perp}^{\dagger} - P(M_{\perp}^{\dagger}M_{\perp})$
Cap.	Isolate transverse and longitudinal magnon modes
App. St.	Explore magnetic field dependence of longitudinal magnons near quantum critical point
S.H. Do et al, in preparation	

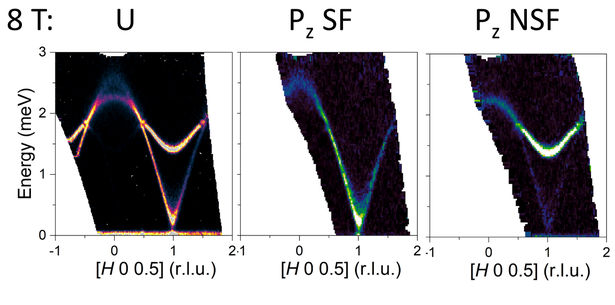

Inelastic neutron scattering on a quantum magnet at 8 Tesla magnetic field, obtained using unpolarized (left panel) and polarized neutrons (center and right panels). Polarization provides detailed information on the nature of interacting magnetic excitation modes.

Isolate nuclear coherent with isotope incoherent scattering

HYSPEC

Sc. A.	Condensed matter
Sc. Ex.	$Fe_{1+y}Te_{0.55}Se_{0.45}$ single crystal, Δy~0.03
Cap. Fam.	Explore magnetic scattering
M-B	$(P\cdot M_{\perp}^{\dagger})M_{\perp} + (P\cdot M_{\perp})M_{\perp}^{\dagger} - P(M_{\perp}^{\dagger}M_{\perp})$
Cap.	Measure only magnetic scattering using spin-flip channel
App. St.	Measure model-matchable magnetic INS for slightly different Fe doping samples
Y. Li et al, *Nature Materials* **20** 1221 (2021)	

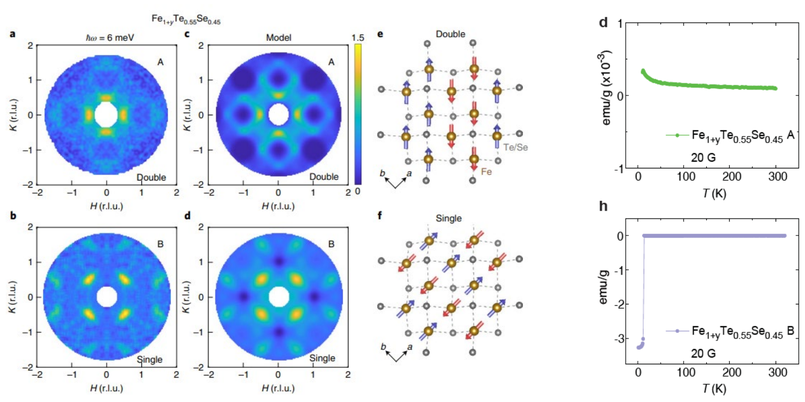

Top row A: Magnetic phase. **Bottom row B:** Superconducting phase.
a,b, Magnetic neutron scattering (P||Q, spin-flip channel, where P is neutron spin polarization and Q is wave vector transfer) measured at 6±1 meV energy transfer where the resonance mode is observed in (b).
c,d, Model fit using the short-range spin correlations model.
e,f, Illustration of the Fe–Te/Se lattice and spin arrangements for the two magnetic patterns.
d,h, Resistivity of the magnetic and superconducting phases, respectively

[1]S. V. **Maleev,** V. G. Bar'yaktar, and R. A. Suris, The scattering of slow neutrons by complex magnetic structures Sov. Phys. Solid State 4, 2533 (1963)
[2]M. **Blume**, Polarization effects in the magnetic elastic scattering of slow neutrons, Phys. Rev. 130, 1670 (1963).

OAK RIDGE National Laboratory | HIGH FLUX ISOTOPE REACTOR | SPALLATION NEUTRON SOURCE

Oak Ridge National Laboratory is managed by UT-Battelle LLC for the US Department of Energy

U.S. DEPARTMENT OF ENERGY | Office of Science

Polarized Neutron Reflectometry

SHUG 2023, Polarization Town Hall

Timothy Charlton, Valeria Lauter

Polarized neutron reflectometry (PNR) as a unique tool that provides simultaneously high-resolution depth profile of chemical composition and of the in-plane magnetization vector and, thus, effectively probes structure and magnetization at buried interfaces and complex magnetic structures. At ORNL, the Magnetism Reflectometer (MR) is operational since 2008. MR is a time-of-flight instrument with wavelengths band of 2.5 - 12.5 A and polarization of 98.5 - 99% of the neutron beam.

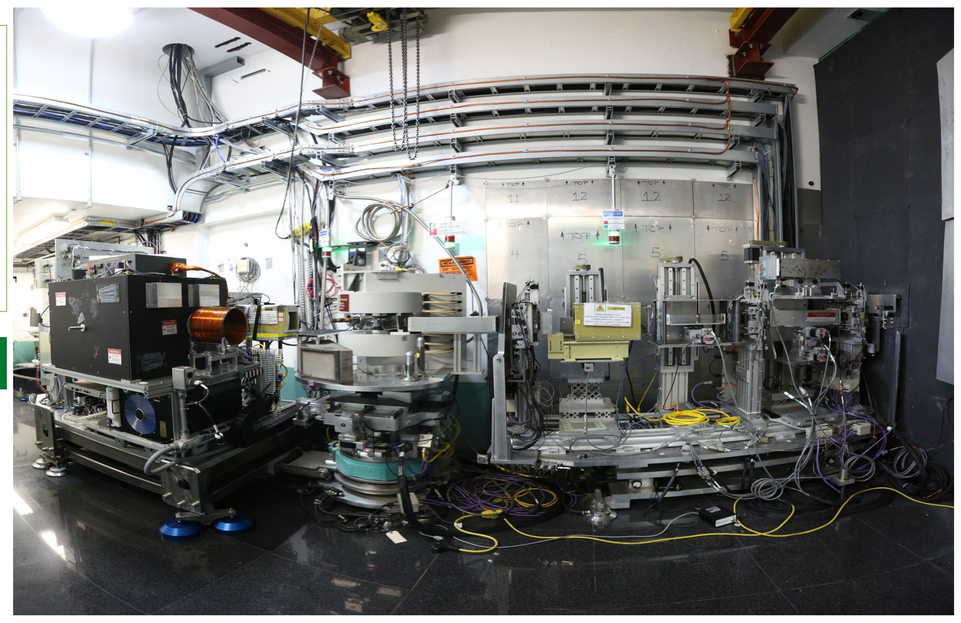

POLARIZED NEUTRON REFLECTOMETRY

- Non-destructive access to distribution of the magnetic induction along the surface normal
- Access to the lateral magnetic domain distribution
- Direct observation of anti-ferromagnetic and spiral magnetization alignments.
- Improved sensitivity in soft matter or any non-magnetic layered systems with the use of a magnetic reference layer

Reflectometry Geometry with Polarized Neutrons

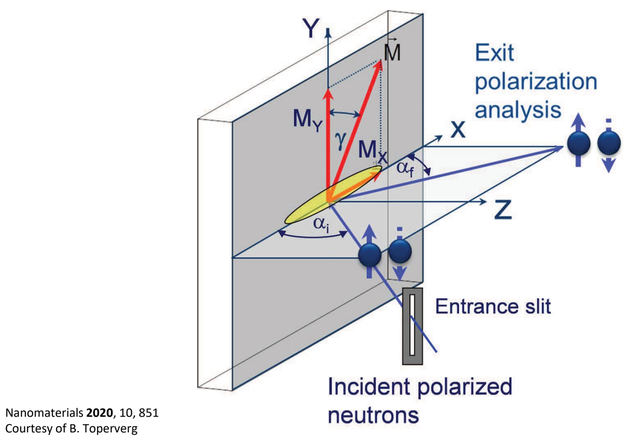

Nanomaterials **2020**, 10, 851
Courtesy of B. Toperverg

Schematic of PNR experiment with polarization analysis along the Y-axis. The ellipsoid indicates the coherence volume of neutrons defined by the beam divergence and the wavelength range.

PNR measures four reflectivities $R^{\pm,\mp}(Q)$ by changing the polarization direction of the of the incident beam and by analyzing the polarization of the reflected beam.

FFT's don't work here. Must solve Schrodinger's EQ exactly.

In general, $R^{\pm,\mp}(Qz)$ is the Fourier transform of the corresponding nuclear and magnetic scattering length density profiles $Nb_n(z)$ and $Nb_m(z)$ in the Z-direction, and N is the nuclear number density.

$$\left[\nabla^2 + \frac{2m_n}{\hbar^2}(E-V)\right]\psi(y) = 0$$

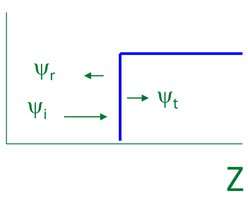

$$V(z) = \frac{2\pi\hbar^2}{m_n}\sum_{i=1}^{layers} N_i b_i \mp \mu_n \cdot B_i$$

$$C = m_n\mu_n/2\pi\hbar^2 = 2.31\times10^{-4}\,\mathrm{nm^{-2}T^{-1}}$$

Non-spin-flip reflectivity:

$R^{++} = 1/4|(r^+ + r^-) + (r^+ - r^-)\cos\gamma|^2$,

$R^{++} = 1/4|(r^+ + r^-) - (r^+ - r^-)\cos\gamma|^2$

Spin-flip reflectivity:

$R^{+-} = R^{-+} = 1/4|\,r^+ - r^-\,|^2 \sin^2\gamma$,

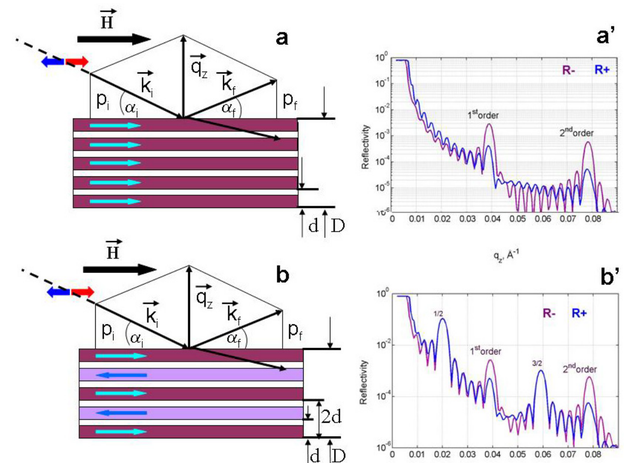

a) **Multilayer (ML) Fe/Cr on sapphire: R+ and R− reflectivity profiles as a function of momentum transfer q_z**; positions of the Bragg peaks are determined by the bilayer thickness d, the Kiessig fringes are due to the total film thickness D.
b) **ML in a remanent external magnetic field resulting in the opposite alignment of the magnetization vectors in the alternating magnetic layers**. b) R^+ and R^- have ½ and 3/2 - order Bragg peaks additional to ones in Fig.a, they are determined by the doubling of the magnetic part of the scattering length density profile.

Magnetism Reflectometer Examples: Half Polarized Reflectometry Configuration (1 polarizer 1 flipper)

Half Polarized Configuration (1 polarizer 1 flipper,)	
Sc. A.	Condensed matter, Soft- matter with the use of a magnetic reference layer
Cap. Fam.	Explore Structure and Magnetism
Cap.	Measure small variation in the magnetic distribution under different conditions.
App. St.	Extract the structure and the in-plane magnetization vector distribution as a function of depth.

Unconventional interlayer exchange mechanism via chiral phonons in synthetic magnetic oxide heterostructures

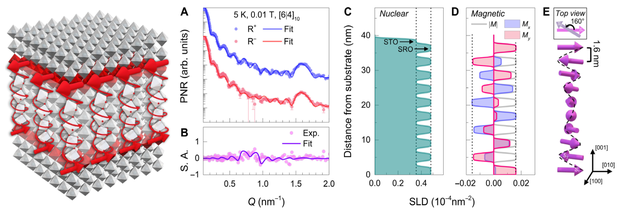

Chiral phonons in artificial oxide superlattices mediate interlayer exchange interaction across a nonmagnetic insulator, leading to a spiral spin structure

Jeong *et al.*, *Sci. Adv.* **8**, eabm4005 (2022)
Jeong *et al.*, *Small Methods*, accepted for publication (2023)

Signatures of superconducting triplet pairing in Ni–Ga-bilayer junctions

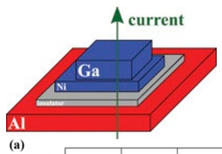

Sketch of the Al/insulator [Al_2O_3 (/EuS)]/Ni–Ga junction. The Al and Ga electrodes are intrinsically superconducting, while proximity effects additionally turn the intrinsically weakly ferromagnetic Ni film into a superconducting one.

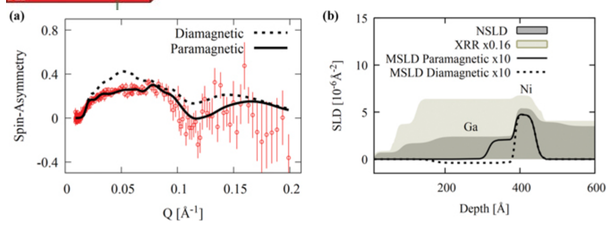

PNR results for the Ni (5.6 nm)–Ga (25 nm) bilayer delivered information about the structure and magnetization of this interface, and detected a paramagnetic Meissner response in Ga, which revealed that the proximity-coupled bilayer induces superconducting triplet pairings around the Ni–Ga interface.

Andreas Costa et al New J. Phys. ***24*** *033046 (2022)*

In operando PNR: Spin Seebeck effect in YIG on GGG

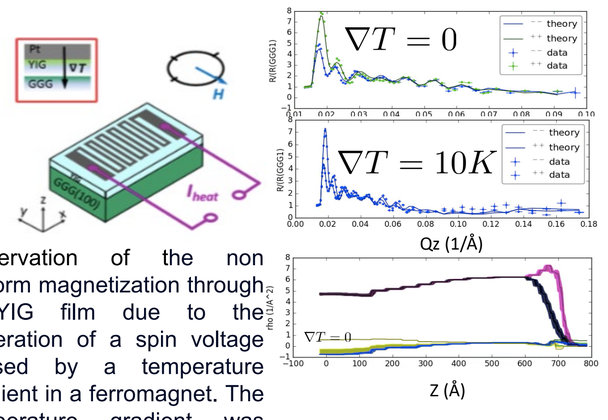

Observation of the non uniform magnetization through a YIG film due to the generation of a spin voltage caused by a temperature gradient in a ferromagnet. The temperature gradient was controlled through a resistive wire deposited on the YIG surface. The reflectivity signal was then separated by a hybrid model.

J.F.K.Cooper et al, PRB 96,104404(2017)
E. Guo et al, Phys Rev X 6, 031012 (2016)

Magnetism Reflectometer Examples: Full Polarized Reflectometry with Off-specular Scattering Configuration (2 polarizers 2 flippers)

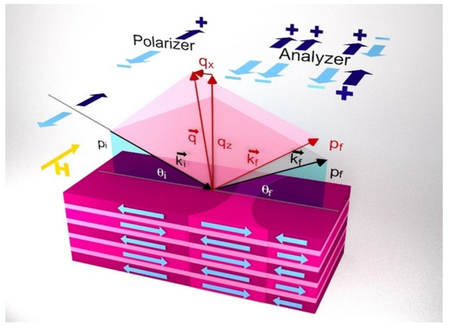

Schematic of PNR experiment with Off-Specular scattering and polarization analysis

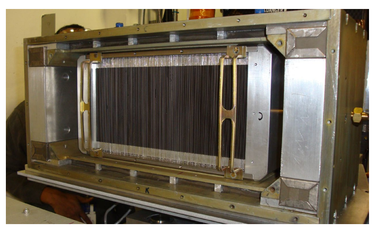

FAN analyzer

V G Syromyatnikov et al J. Phys.: Conf. Ser. ***528*** *012021 (20214)*

Non-collinear magnetization vector reversal in organic spin-valve $SrTiO_3$//$LaSrMnO_3$/ (PFO)/Co/Ag

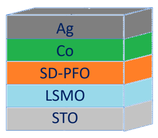

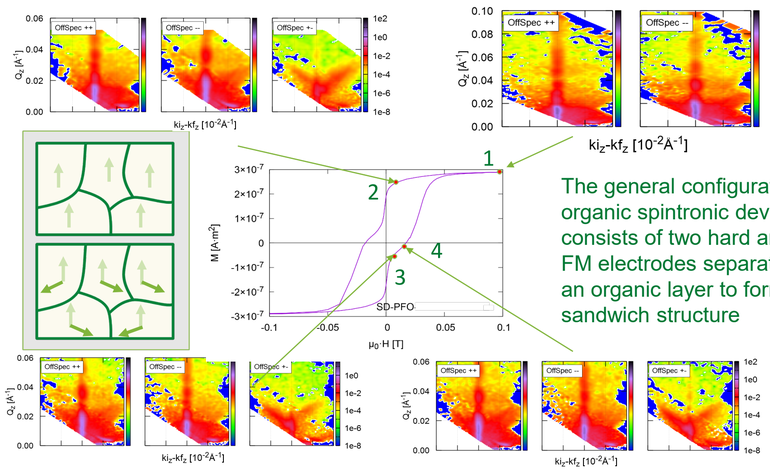

The general configuration of organic spintronic device consists of two hard and soft FM electrodes separated by an organic layer to form a sandwich structure

PNR and Physical Properties Measurements System (PPMS) experiments. PNR results indicated that the optimized $La_{0.7}Sr_{0.3}MnO_3$ (LSMO) and Co layers are ferromagnetic (FM) so that they can act as good soft and hard ferromagnetic electrodes in the devices.

J Keum et al., in preparation, 2023

Magnetic Materials with tunable Properties: Magnetization configurations in continuous and patterned FeRh films

FeRh films *continuous*

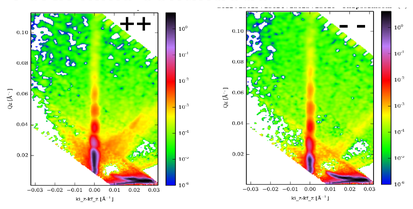

FeRh features a temperature- or field-induced metamagnetic transition from the antiferromagnetic order (AF) to the ferromagnetic order (FM) that occurs at 370 K at zero magnetic field. Strong spatial confinement and strain have a significant impact on the phase coexistence and reversal dynamics of the transition.

FeRh 6.7 μm stripes on MgO 450 K 5mT

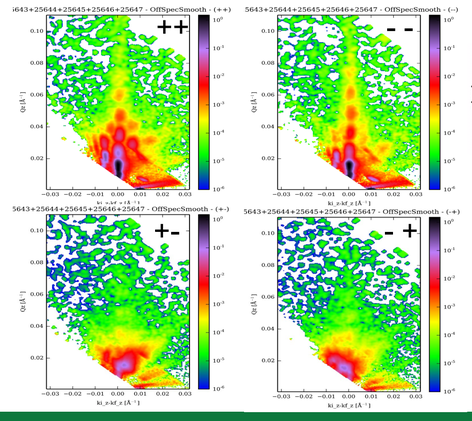

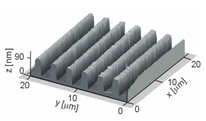

PNR established that a residual positive moment in thin films in the AF phase originates from interfaces, most likely a result of strain and disorder. The reflectivity fitting of stripes suggest behavior similar to a continuous film, but with addition of defects throughout the depth of the film, likely at the wire edges, which influence the FeRh phase and transition.

Sheena Patel et al., in preparation, 2023

High resolution boosted by Larmor labeling of neutron spin

Fankang Li[1], K. Burrage[1], F. Funama[1], L. Crow[1], M. Matsuda[2], K. Hong[3], M. Manley[4], R. Hermann[4], O. Delaire[5]

1. Neutron Technologies Division, ORNL. 2. Neutron Scattering Division, ORNL. 3. Center for Nanophase Materials Sciences, ORNL. 4. Materials Science and Technology Division, ORNL. 5. Mechanical Engineering and Materials Science, Duke University.

Conventional diffractometer

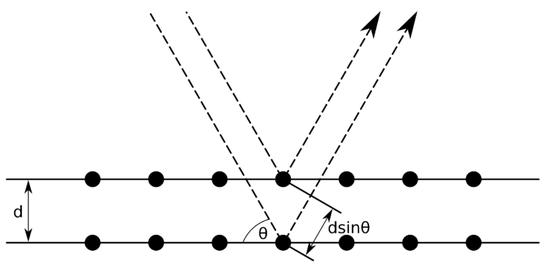

$$n\lambda = 2d\sin\theta$$

$$\frac{\Delta d}{d} = \sqrt{\left(\frac{\Delta\lambda}{\lambda}\right)^2 + \left(\cot\theta\Delta\theta\right)^2}$$

- Resolution limited by the beam divergence and wavelength spread
- Typical resolution is $\Delta d/d = 10^{-2} - 10^{-3}$

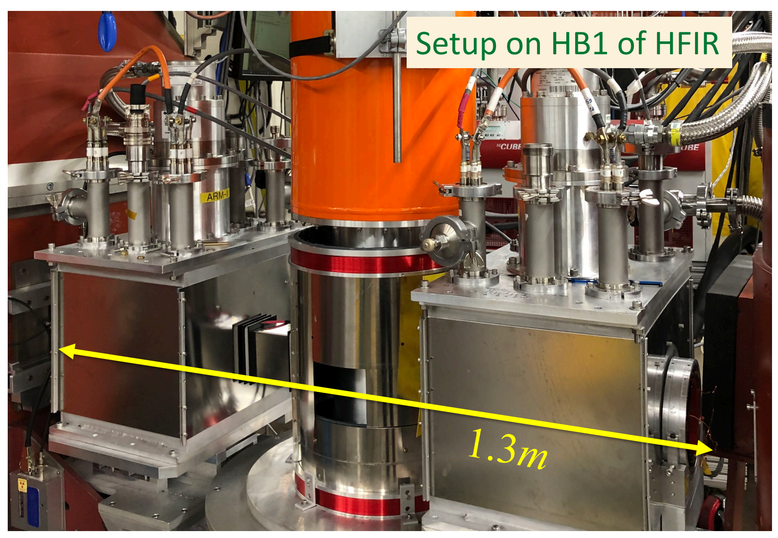

Wollaston prism

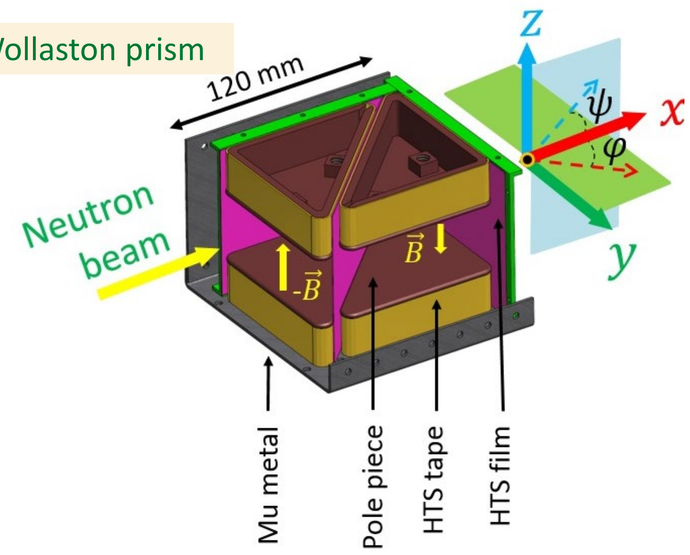

Principle of Larmor diffraction

Bragg's Law: $k_{i,\perp} = \frac{2\pi}{d}$

Larmor phase: $\Phi = \frac{\gamma_N mBL}{hk_{i,\perp}}$

$$\Phi = \frac{\gamma_N mBLd}{2\pi h}$$

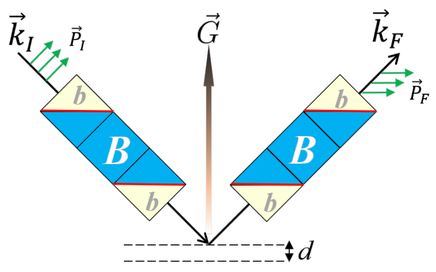

- The *d* spacing distribution is encoded into Larmor phase-Fourier transform
- High resolution for d-spacing expansion Δd/d~10^{-6}.
- The tilting angle has to match the crystal plane.

Inelastic Neutron Spin Echo

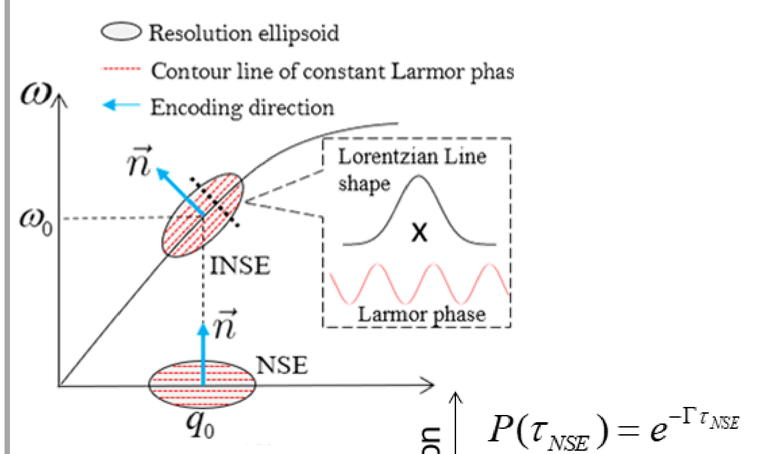

$$P(\tau_{NSE}) = e^{-\Gamma\tau_{NSE}} = e^{-\frac{\tau_{NSE}}{\tau_{lifetime}}}$$

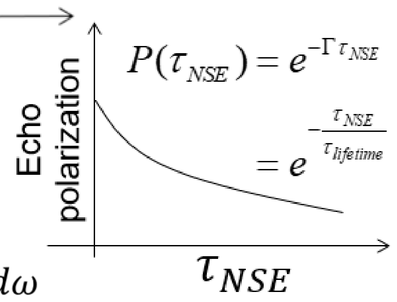

$$P \propto \int S(\omega)\cos(\omega\tau)d\omega$$

Spin Echo Small Angle Neutron Scattering (SESANS)

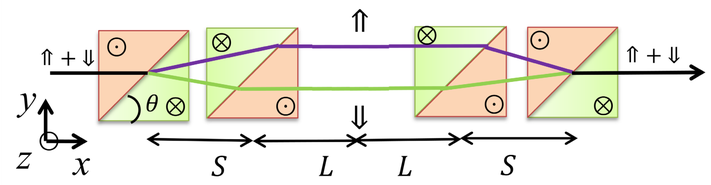

1. Works in real space.
2. Length scale can be extended beyond 1um.
3. Is not sensitive the multiple scattering.
4. Measures1D correlation function.

35% Polymethyl methacrylate (PMMA)

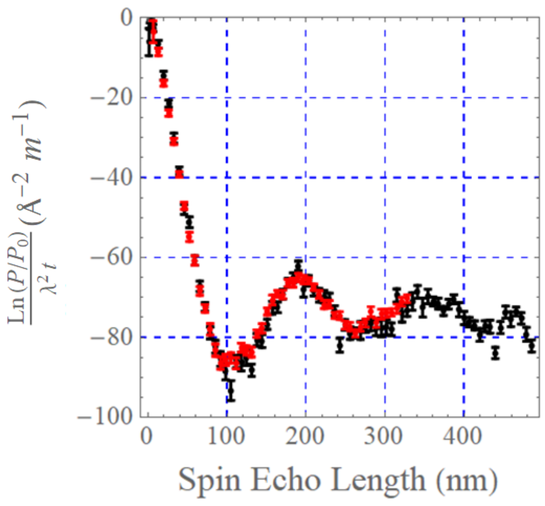

Data interpretation-a Fourier transform

$$P(\Phi) = \int f(\frac{\Delta d}{d})\cos(\Phi\frac{\Delta d}{d})d(\frac{\Delta d}{d})$$

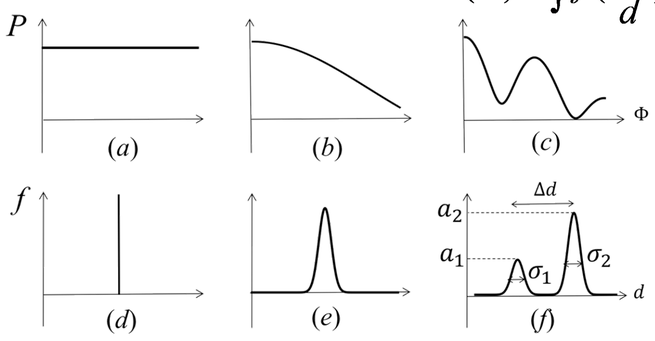

Phonon lifetime of Bismuth

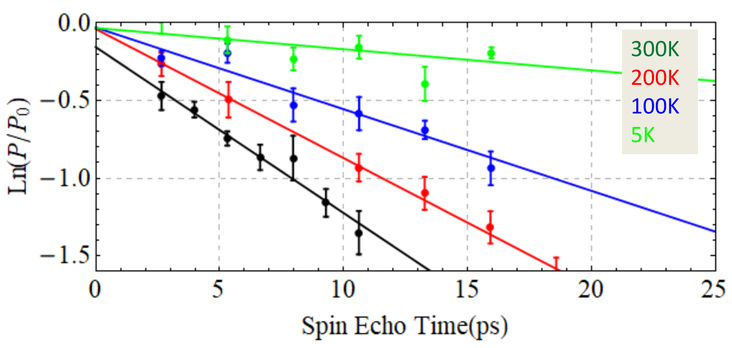

Temperature(K)	Linewidth from simulation (μeV)	Linewidth from HB1 (μeV)
100	15	25.65±7.06
200	32	45.79±3.57
300	52.5	61.41±7.86

An energy resolution of <10μeV has been achieved to measure both the phonon energy shift and linewidth of Bismuth

Larmor diffraction for lattice distortion and expansion measurements

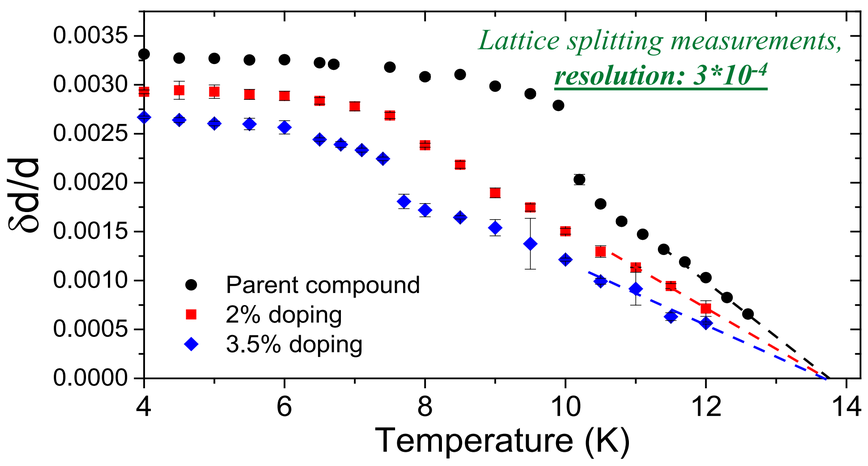

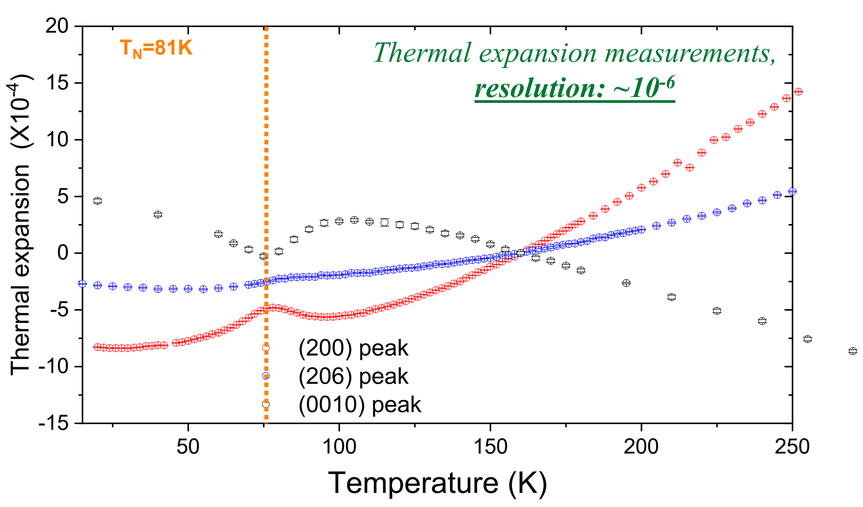

Grüneisen Parameter Measurement of GaSb

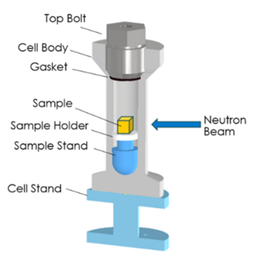

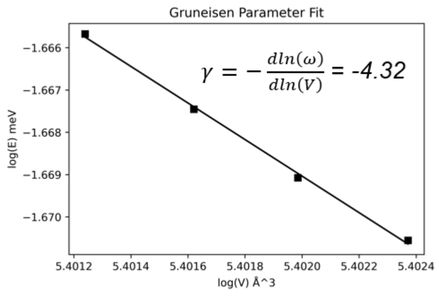

Capable of measuring the Grüneisen parameter with large sample (8 cm^3) and low pressure (1kbar) due to the high energy resolution of INSE.

Nanoporous alumina

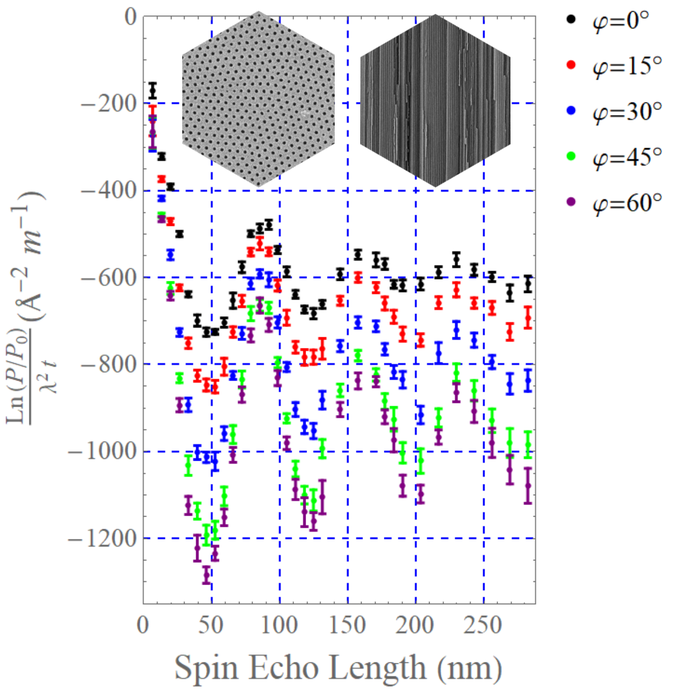

References

Li, F. et al., (2017). *Scientific Reports* **7**, 865.
Li, F. et al., (2014). *Rev. Sci. Instrum.* **85**, 053303.
Li, F. et al., (2014). *J. Appl. Cryst.* **47**, 1849-1854.
Li, F. et al., (2018). *J. Appl. Cryst.* **51**, 584-590
Please visit: https://fankangli.ornl.gov/

This work was supported by the US Department of Energy, Office of Science, Office of Basic Energy Sciences, Early Career Research Program Award (KC0402010), under Contract No. DE-AC05- 00OR22725.

Development of Spherical Neutron Polarimetry for HFIR and Beyond

Chenyang Jiang[1], Nicolas Silva[1], Jacob Tosado[1], Tianhao Wang[1], Masaaki Matsuda[2], Barry Winn[2], Lowell Crow[1]

[1]Neutron Technologies Division, Oak Ridge National Laboratory

[2]Neutron Scattering Division, Oak Ridge National Laboratory

Motivation

- Distinguish between polarization rotation and depolarization
- Study complex magnetic materials
  - Spin-topological matter
  - Magneto-electric crystals
  - Superconductors, etc.

Principle

- Decouple the incoming and outgoing neutron polarization
  - Zero-field chamber
  - Combination of adiabatic and non-adiabatic transitions to control neutron polarization

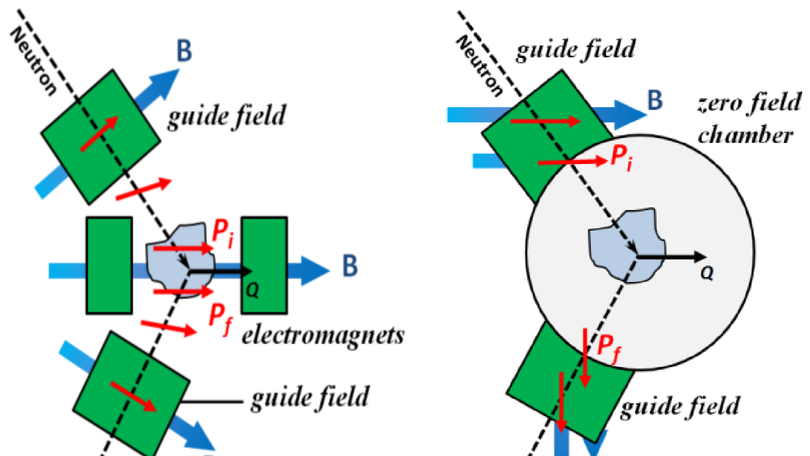

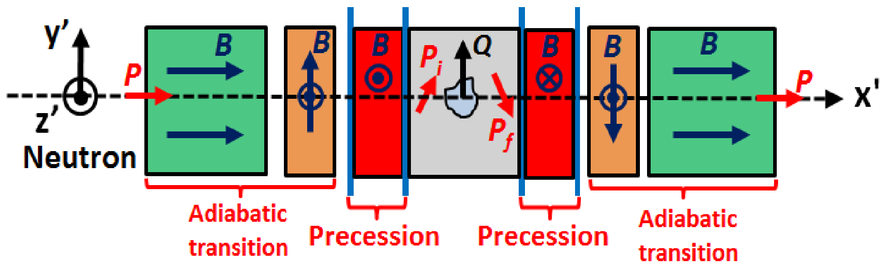

Portable High-Tc Polarization Analysis Device (PHitPAD)

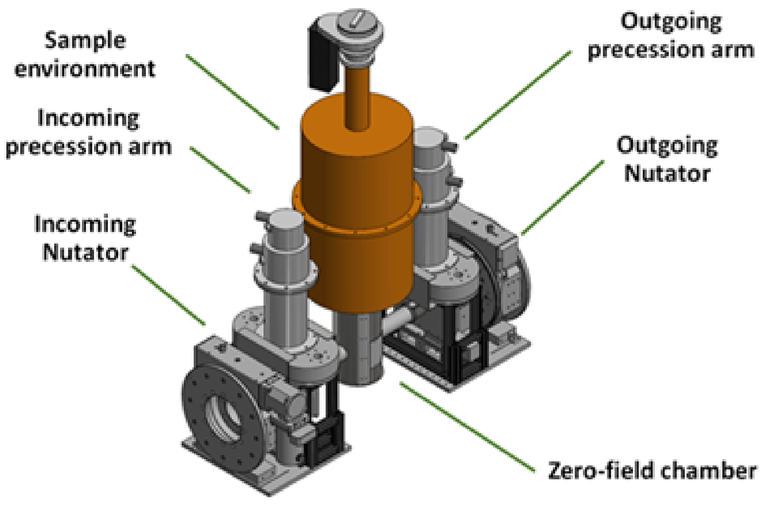

Essential components

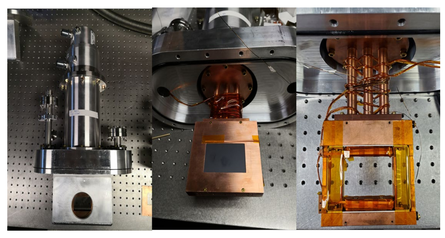

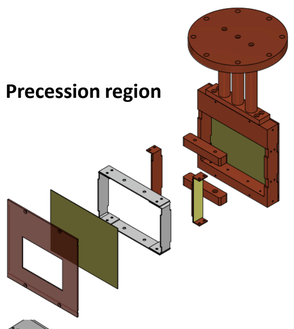

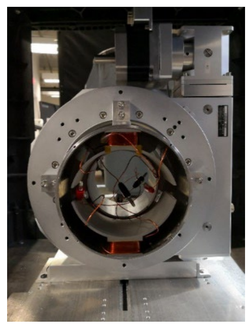

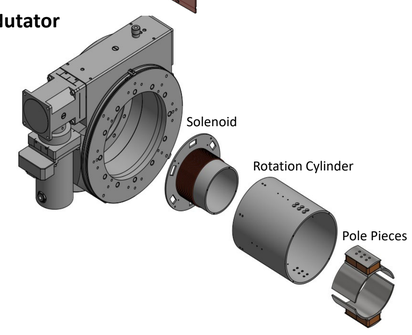

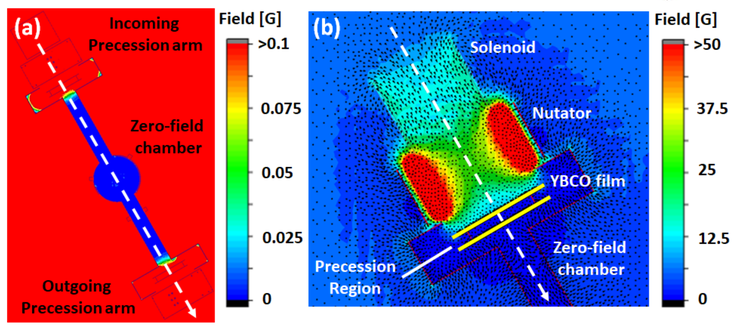

Setup and Test at HFIR HB-1

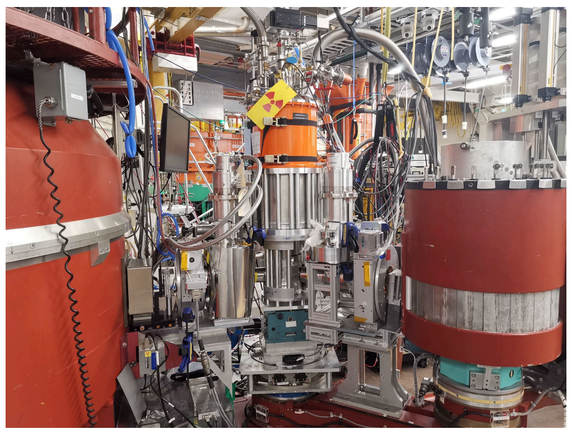

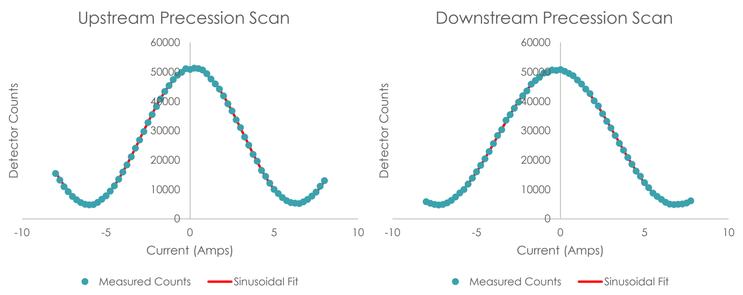

Sample	Peak Type	Theoretical Polarization Matrix	Measured Polarization Matrix
Silicon	Nuclear (1,1,1)	$\begin{bmatrix}1&0&0\\0&1&0\\0&0&1\end{bmatrix}$	$\begin{bmatrix}0.883\pm0.003 & 0.034\pm0.002 & -0.022\pm0.002\\ 0.019\pm0.002 & 0.883\pm0.003 & -0.012\pm0.002\\ 0.048\pm0.002 & 0.022\pm0.002 & 0.854\pm0.003\end{bmatrix}$
Bismuth Ferrite $BiFeO_3$	Magnetic (0.5,0.5,0.5)	$\begin{bmatrix}-1&0&0\\0&0&0\\0&0&0\end{bmatrix}$	$\begin{bmatrix}-0.829\pm0.014 & -0.015\pm0.010 & 0.005\pm0.011\\ 0.025\pm0.010 & 0.031\pm0.010 & 0.021\pm0.011\\ 0.022\pm0.011 & 0.0368\pm0.011 & -0.012\pm0.011\end{bmatrix}$
CYCO $Ca_2Y_2Cu_5O_{10}$	Nuclear (0,0,2)	$\begin{bmatrix}1&0&0\\0&1&0\\0&0&1\end{bmatrix}$	$\begin{bmatrix}0.828\pm0.009 & -0.005\pm0.007 & 0.027\pm0.007\\ 0.027\pm0.007 & 0.837\pm0.009 & -0.027\pm0.007\\ -0.030\pm0.007 & 0.012\pm0.007 & 0.831\pm0.009\end{bmatrix}$
CYCO $Ca_2Y_2Cu_5O_{10}$	Magnetic (0,0,1)	$\begin{bmatrix}-1&0&0\\0&1&0\\0&0&-1\end{bmatrix}$	$\begin{bmatrix}-0.842\pm0.014 & -0.003\pm0.006 & -0.006\pm0.006\\ 0.017\pm0.006 & 0.834\pm0.004 & 0.027\pm0.006\\ 0.001\pm0.006 & -0.020\pm0.006 & -0.806\pm0.013\end{bmatrix}$

SNP on a Chiral magnet sample

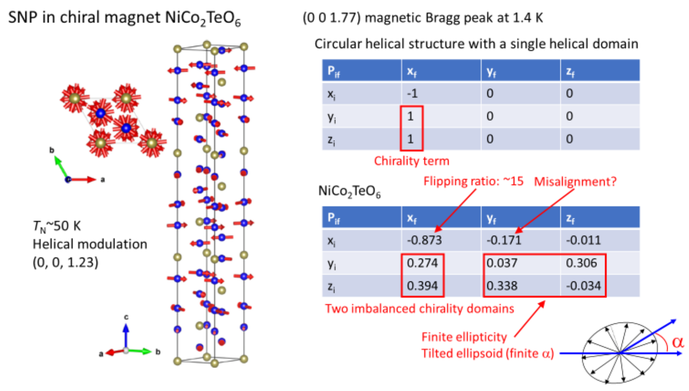

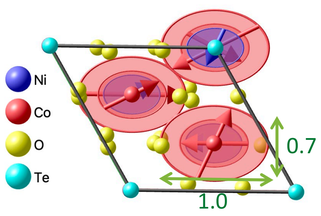

- chirality domain ratio ~ 0.685 : 0.315
- ellipticity 1.0 : 0.7
- α ~ 45°

Towards time-of-flight instruments

- No SNP device for time-of-flight instruments to date
- Neutron polarization precession is energy dependent
  - Extremely difficult to align different wavelength neutron polarization
- HYSPEC at SNS
  - Direct geometry spectrometer
  - Monochromatic incident beam
  - Polychromatic scattered beam
- SNP on HYSPEC
  - Only need to focus on the scattered beam side
  - Rely on adiabatic transition to align the neutron polarization to the analyzer

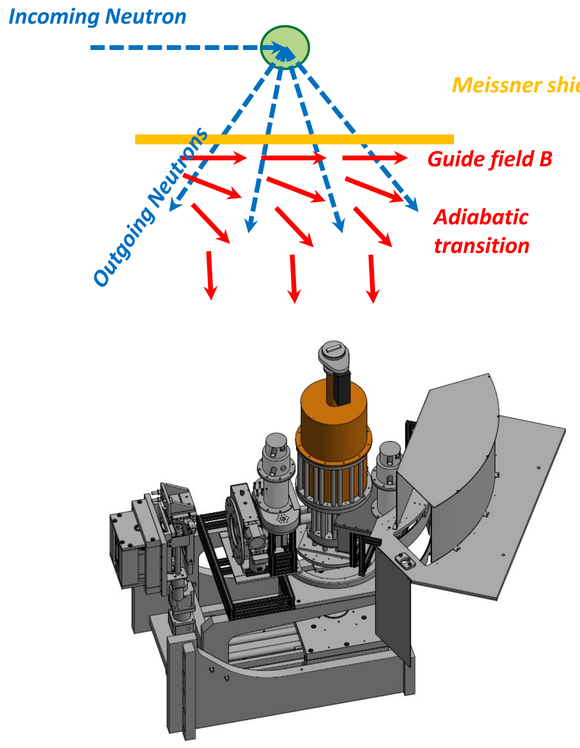

Summary

- PHitPAD in HFIR user program
- User experiments scheduled on HB-1
- Design of SNP on HYSPEC is underway

Acknowledgements: Research was performed at HFIR and SNS, two DOE Office of Science User Facilities. Parts of the research were supported by ORNL's Laboratory Directed Research and Development (LDRD) program. C.J. acknowledges the support of U.S. DOE BES Early Career Award No. KC0402010, under Contract DE-AC05-00OR22725.

Polarized Neutron applications for Biology, Soft Matter, & Chemistry

25th National School on Neutron & X-Ray Scattering, 2023

Longitudinal 1 at MACS (NCNR)

Science Area	Chemistry
Science Example	Partially deuterated Methanol
Capability Family	Separate coherent and spin-incoherent scattering
Relevant terms	$PN^{\dagger}N - \frac{1}{3}PI_{si}$
Capability	Separate dynamic structure factors in a wide Q range
Application Statement	Sensitive measurement of weak coherent scattering

W. Chen *et al*, "Wide-angle polarization analysis on the multi-axis crystal spectrometer for the study of collective and single particle dynamics of methanol at its prepeak," *Physica B: Condensed Matter* **564** 166 (2019)

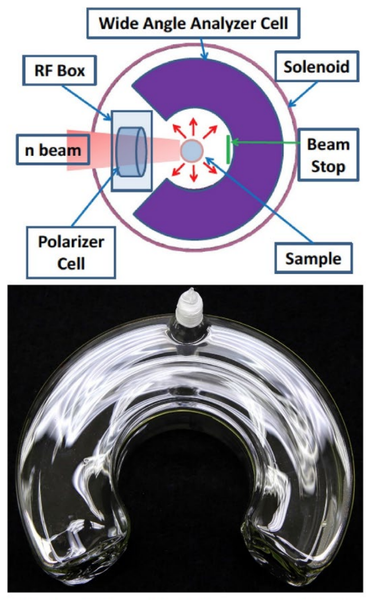

Fig. 1. Top view of the layout of the spin filter apparatus in the MACS sample area (top picture). Cold incident neutrons are polarized by a polarized ^{3}He cell that is located in an RF end-compensated solenoid surrounded by an aluminum shielding box and focused at the sample position. After scattering from the sample, neutrons are spin-analyzed by a horseshoe-shaped wide angle ^{3}He analyzer (bottom picture) and detected with a 20-detector bank system.

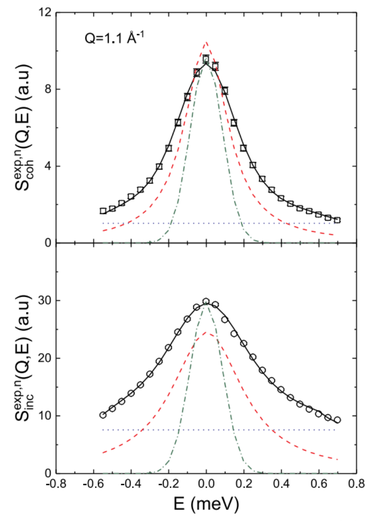

Fig. 3. Fit of the experimental data according to Eq. (13) at Q = 1.1 Å^{-1}. The symbols are experimental data, the continuous black line is the fit; the red dashed, blue dotted, and green dash-dotted lines represent the Lorentzian function before convolution, the linear background, and the height scaled resolution function respectively. (For interpretation of the references to colour in this figure legend, the reader is referred to the web version of this article.)

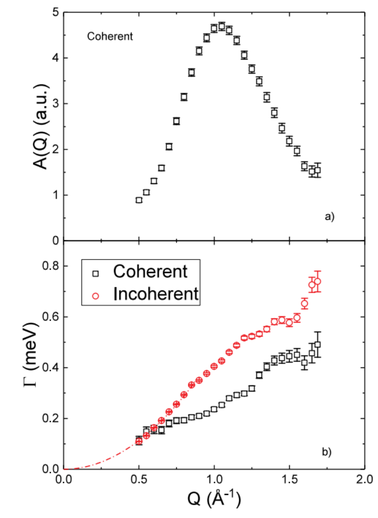

Fig. 4. a) The area of the coherent spectra. Notice the location of the maximum in correspondence of the prepeak. b) The FWHM values obtained from the fitting of the coherent and incoherent spectra using Eq. (13). The dash-dot red line represents the fit of the incoherent spectral width to a Fickian diffusion model in the range up to Q = 0.85 Å^{-1}. Notice how the results of the coherent signal do not follow the Q^2 behavior of the Fickian diffusion and a slowing down of the dynamics can be observed in correspondence of the prepeak. (For interpretation of the references to colour in this figure legend, the reader is referred to the web version of this article.)

Longitudinal 1 at SANS instrument TAIKAN (BL15, J-PARC)

Science Area	Chemistry
Science Example	Colloidal particles of either TBP/$(HNO_3)_x$ or PtCl6(BEHU.H)$_2$
Capability Family	Separate coherent and spin-incoherent scattering
Relevant terms	$PN^{\dagger}N - \frac{1}{3}PI_{si}$
Capability	Separate structure factors at low Q
Application Statement	Sensitive measurement of weak coherent scattering

T. Okudaira *et al*, "Polarization analysis for small-angle neutron scattering with a ^{3}He spin filter at a pulsed neutron source," *J. Appl. Cryst.* **54** 548 (2021)

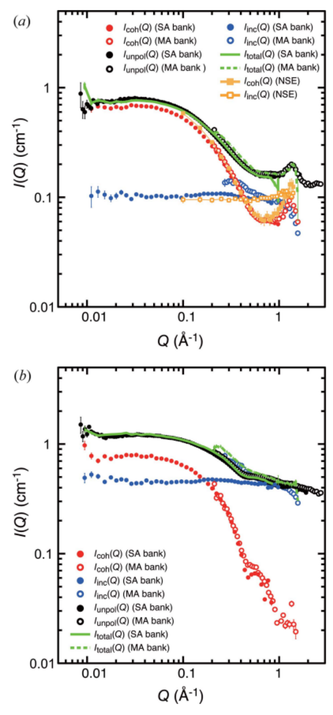

Figure 4
Double logarithmic plots of the SANS profiles obtained for the colloidal particle dispersions of (*a*) TBP/$(HNO_3)_x$ and (*b*) $PtCl_6(BEHU{\cdot}H)_2$ complexes (samples 1 and 2). The NPA results, *i.e.* $I_{coh}(Q)$ (red closed and open circles) and $I_{inc}(Q)$ (blue closed and open circles), are plotted together with their sum, $I_{total}(Q)$ (green solid and dashed lines). SANS profiles obtained using an unpolarized incident neutron beam are indicated by black closed and open circles. The NPA results obtained using an NSE spectrometer for sample 1 only are indicated in (*a*) by orange closed and open squares for $I_{coh}(Q)$ and $I_{inc}(Q)$, respectively, with an intensity scale factor of approximately 0.9. The abbreviations SA and MA denote the small-angle and middle-angle detector banks, respectively.

Longitudinal 1 at D7 (ILL)

Science Area	Chemistry
Science Example	Heavy Water
Capability Family	Separate coherent and spin-incoherent scattering
Relevant terms	$PN^{\dagger}N - \frac{1}{3}PI_{si}$
Capability	Separate dynamic structure factors in a wide Q range
Application Statement	Observe collective fluctuations at mesoscales

A. Arbe *et al*, "Coherent structural relaxation of water from meso- to intermolecular scales measured using neutron spectroscopy with polarization analysis," *Physical Review Research* **2** 022015(R) (2020)

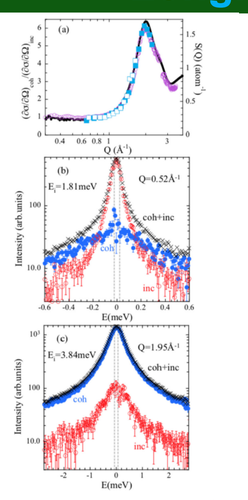

FIG. 1. (a) The ratio between coherent and incoherent differential cross sections $(\partial\sigma/\partial\Omega)_{coh}/(\partial\sigma/\partial\Omega)_{inc}$ of D_2O at 298 K (hollow dots) as a function of Q obtained by diffraction with PA (D7 at the Institute Laue Langevin, Grenoble, France) [9], and calculated from MD simulations (solid line, see SM [19]). The figure also includes the additional y-axis scale (right) corresponding to $S(Q) = (\partial\sigma/\partial\Omega)_{coh}/[\sigma_{coh}/(4\pi)]$ where $\sigma_{coh}/(4\pi) = \lim_{Q\to\infty}(\partial\sigma/\partial\Omega)_{coh}$. Squares represent the QENS amplitudes (rescaled to match the D7 data) obtained from the application of the model to the LET results (filled, E_i = 3.84 meV; empty, E_i = 1.81 meV). (b) and (c) Comparison of the coherent and incoherent dynamical structure factors measured by LET on D_2O at 295 K at the Q values indicated, and the total spectra (coherent + incoherent). Vertical dotted lines represent the resolution FWHM.

Science Area	Chemistry
Science Example	Protic Ionic Liquids
Capability Family	Separate spin-incoherent from coherent scattering
Relevant terms	$PN^{\dagger}N - \frac{1}{3}PI_{si}$
Application Statement	Compare coherent scattering to simulation for both structure and QENS

T. Burankova *et al*, "Linking Structure to Dynamics in Protic Ionic Liquids: A Neutron Scattering Study of Correlated and Single-Particle Motions," *Scientific Reports* **8**, 16400 (2018)

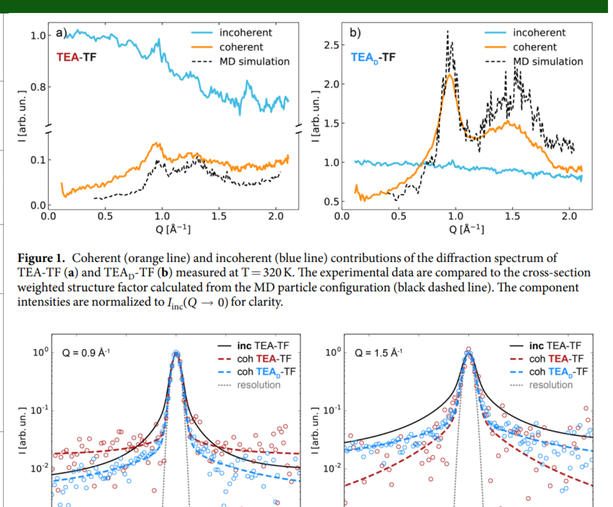

Figure 1. Coherent (orange line) and incoherent (blue line) contributions of the diffraction spectrum of TEA-TF (**a**) and TEA_D-TF (**b**) measured at T = 320 K. The experimental data are compared to the cross-section weighted structure factor calculated from the MD particle configuration (black dashed line). The component intensities are normalized to $I_{inc}(Q \to 0)$ for clarity.

Figure 6. Coherent dynamic structure factor of TEA-TF (dashed red line) and TEA_D-TF (dashed blue line) at the charge-charge (**a**) and adjacency (**b**) correlation peaks. The incoherent dynamic structure factor of the protonated sample (black solid line) is presented for comparison. The gray dotted line is the resolution linewidth at zero energy transfer for the D7 spectrometer.

DNP / Half at IMAGINE (CG-4D, HFIR)

Sc. A.	Biology
Sc. Ex.	wt*T4L single crystal
Cap. Fam.	Dynamic Nuclear Polarization
M-B	$N^{\dagger}N + I_{si}$
Cap.	Dynamic Nuclear Polarization
App. St.	

J.Pierce et al, *in preparation*

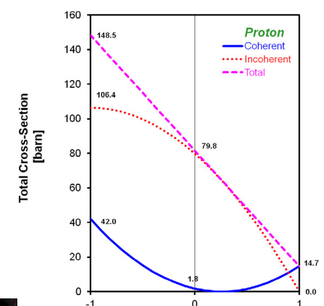

Anti-aligned - Aligned

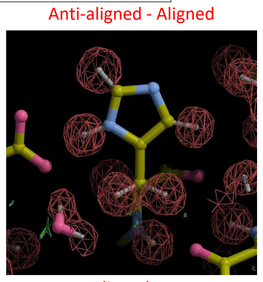

Aligned

Anti-aligned

Unpolarized

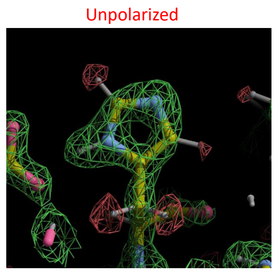

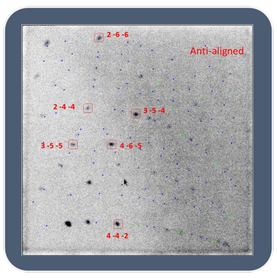

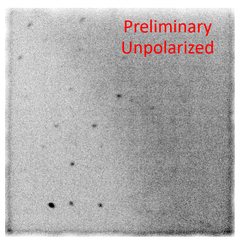

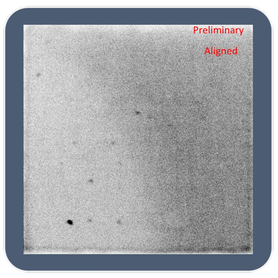

DNP / Half at iMATERIA (BL-20, J-PARC)

Science Area	Biology
Science Example	Hair with water, , follicles aligned vertically
Capability Family	Dynamic Nuclear Polarization (with fast sample exchange)
Relevant terms	$N^{\dagger}N + I_{si}$
Capability	Vary Hydrogen polarization to explore coherent scattering of Hydrogen with different soaking conditions
Application Statement	Determine water distribution in hair

Y. Noda *et al*, "Water distribution in human hair microstructure elucidated by spin contrast variation small-angle neutron scattering," *J. Appl. Cryst* **56** (2023)

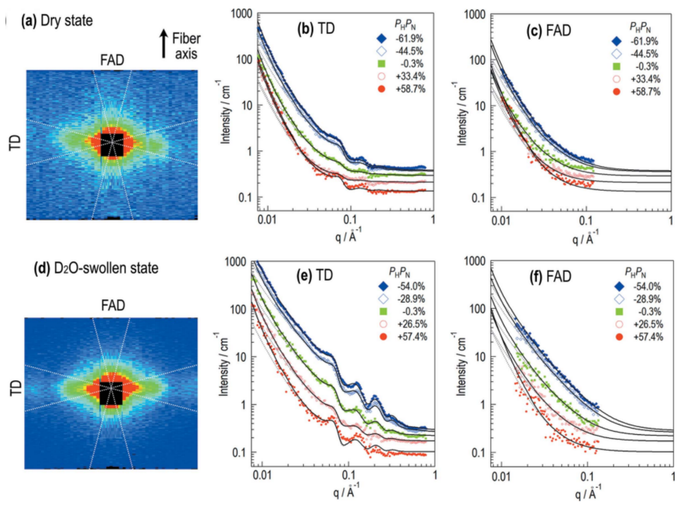

Figure 6
DNP–SANS experimental results. Two-dimensional image of scattered neutron intensity on the small-angle detector bank [(*a*) dry hair at P_HP_N = −61.9%, (*d*) D_2O-swollen hair at P_HP_N = −54.0%], with the neutron wavelength range 3–4 Å. Dotted white lines indicate areas for sector averaging. One-dimensional SANS profiles are shown for dry hair in TD (*b*) and FAD (*c*) and for D_2O-swollen hair in TD (*e*) and FAD (*f*). The horizontal axis is the magnitude of the scattering vector q [= $(4\pi/\lambda)\sin\theta$, where λ is the neutron wavelength and 2θ is the scattering angle]. The solid black and gray dotted curves are numerically calculated profiles with and without considering the smear effect, respectively.

Science Area	Soft Matter
Science Example	Silica-filled Rubber (2 component system)
Capability Family	Dynamic Nuclear Polarization (with fast sample exchange)
Relevant terms	$N^{\dagger}N + I_{si}$
Capability	Vary Hydrogen polarization to explore coherent scattering of Hydrogen in industrial samples
Application Statement	Sample is a new standard utilized to calibrate the DNP system

Y. Noda *et al*, "First Experiment of Spin Contrast Variation Small-Angle Neutron Scattering on the iMATERIA Instrument at J-PARC," *Quantum Beam Sci* **2020**, 33 (2020)

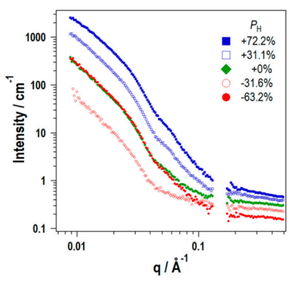

Figure 7. SANS profiles with limited neutron wavelength from 4 Å to 10 Å, for the silica-filled rubber at various P_H.

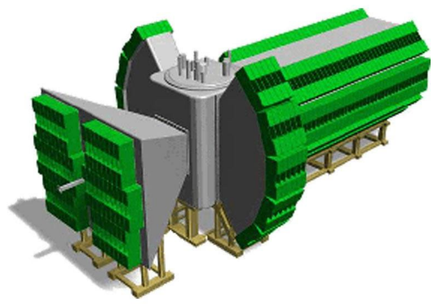

Polarized Neutron applications for Materials & Engineering

25th National School on Neutron & X-Ray Scattering, 2023

Longitudinal 2 Configuration (2 filters, 4 π/2 flippers) Tensor Imaging at CONRAD, HZB (V7, RIP)

Science Area	Materials & Engineering
Science Example	(1) Electric coil, (2) trapped magnetic flux within type-1 superconductor lead
Capability Family	explore magnetic scattering
Larmor	$\vec{\tau} = \vec{\mu} \times \vec{B},\ \omega = -\gamma B$
Capability	Novel tensorial multiplicative algebraic reconstruction technique, with 9 spin polarized neutron imaging measurements
Application Statement	Quantify field magnitude and direction and domain structures, where direct probes cannot access

A. Hilger *et al*, "Tensorial neutron tomography of three-dimensional magnetic vector fields in bulk materials," *Nature Communications* **9**, 4023 (2018)

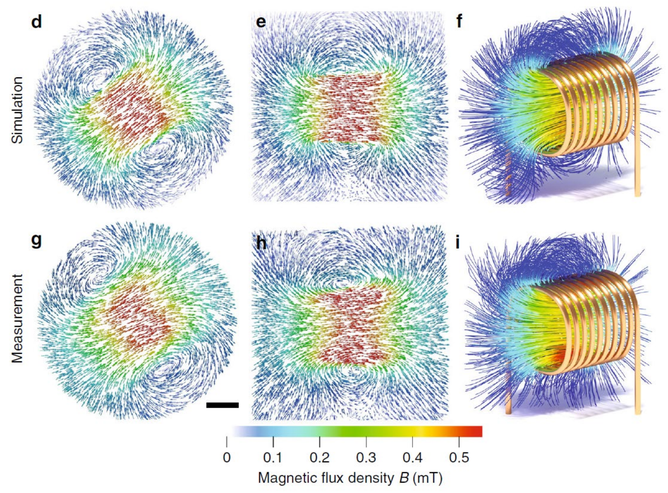

Vectors of the magnetic field produced by an electric coil (including leads). **D)-F)** reconstruction of simulated measurement. **G)-I)** Measured magnetic vector field distribution of the real coil.

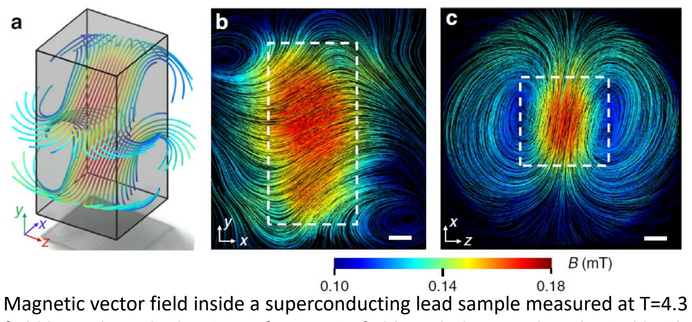

Magnetic vector field inside a superconducting lead sample measured at T=4.3 K. **A)** Some selected magnetic field lines show the location of magnetic field insidethe sample indicated by the cuboid. **B)** in a selected xy plane (silhouette marked by dotted lines). Scalebar, 5 mm. **C)** in a selected yz plane. Scale bar, 5 mm.

Longitudinal 1 Configuration (2 filters, 1 flipper) SANS at NCNR, NG7SANS

Science Area	Materials & Engineering
Science Example	ferromagnetic alloy $Ni_{0.89}V_{0.11}$
Capability Family	explore magnetic scattering
Capability	Isolate magnetic scattering
Application Statement	Identify small magnetic cluster contributions. Azimuthal angle dependence of spin-flip and non-spin flip scattering reveal magnetic contributions at different length scales

K. Hiroi *et al*, "Revealing magnetic correlations in ferromagnetic alloys with polarized SANS," *Journal of Physics, Conference Series* **2481**, 012001 (2023) (PNCMI)

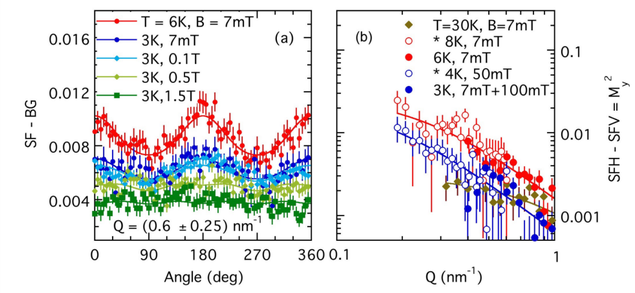

Figure 3: (a) Neutron scattering intensity (spin flip response) vs. azimuthal angle θ collected in the Q range of (0.35-0.85)nm^{-1} at different temperatures T and magnetic fields B. Fits are shown as solid lines using Eq. (2). (b) Magnetic neutron scattering intensity vs. wave vector Q: the spin-flip contrast, SFH-SFV, is shown in small magnetic fields ($B \leq 50$ mT) representing M_y^2 or 1/3 of the total isotropic magnetic response M_{tot}. *Data from lower Q range [12] are included with open symbols. Solid lines follow Eq. (4)

Half Polarized Configuration (1 filters, 1 flipper) Single crystal diffractometer at Heinz Maier-Leibnitz Zentrum, POLI

Science Area	Materials & Engineering
Science Example	ferromagnetic shape memory alloy Ni_2MnGa
Capability Family	separate nuclear and magnetic scattering
Relevant terms	$N^\dagger N + \boldsymbol{M}_\perp^\dagger \boldsymbol{M}_\perp + \boldsymbol{P} \cdot \boldsymbol{M}_\perp^\dagger N + \boldsymbol{P} \cdot \boldsymbol{M}_\perp N^\dagger$
Capability	separate nuclear and magnetic scattering
Application Statement	Follow moment reorientation as a function of compressive stress and magnetic field

Y.B. Ke *et al*, "Unraveling magneto-structural coupling of Ni_2MnGa alloy under the application of stress and magnetic field using in situ polarized neutron diffraction," *Appl. Phys. Lett.* **117,** 081905 (2020)

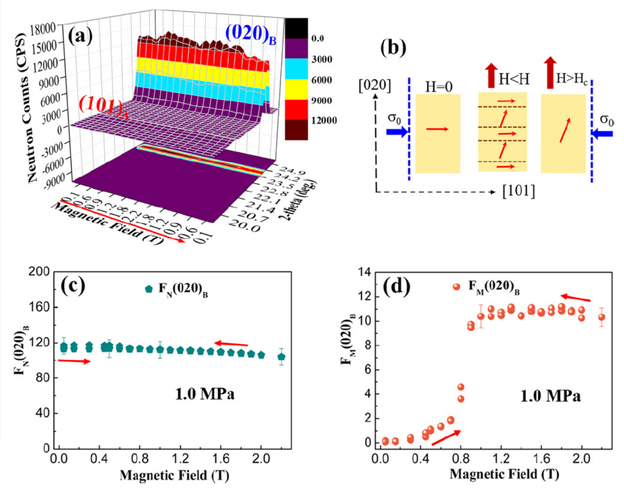

FIG. 3. (a) Change in the one-dimensional integrated peak profiles of $(101)_A$ and $(020)_B$ with spin up neutrons during the application of the magnetic field under a compressive stress of 1.0 MPa. (b) Schematic of the magnetization process driven by the magnetic field under constant stress (σ_0). Variations of (c) the nuclear structure factor F_N and (d) the magnetic structure factor F_M of the $(020)_B$ peak as a function of the magnetic field.

Longitudinal 1 Configuration (2 filters, 0 flipper, non-spin-flip only) Depolarization Imaging at MARS, HFIR CG-1D

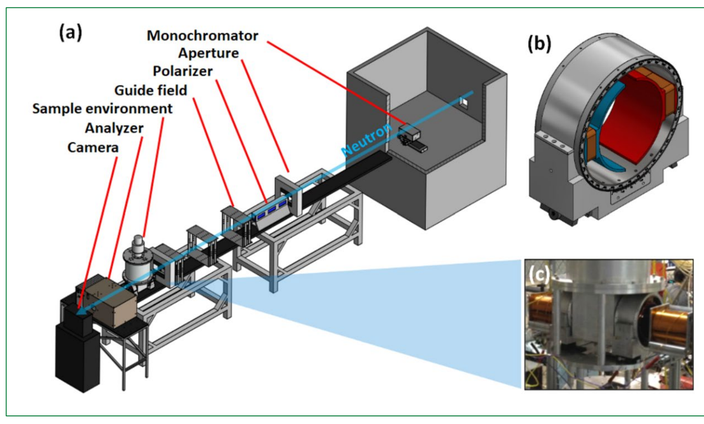

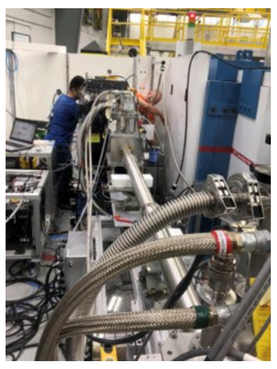

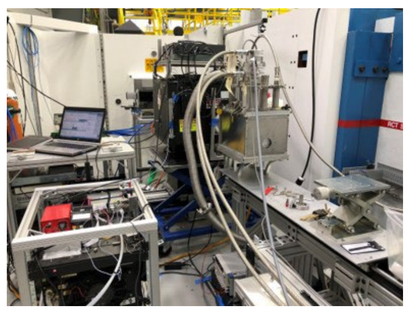

Sc. A.	Materials & Engineering
Sc. Ex.	Cylindrical coil at varying current
Cap. Fam.	Explore Magnetism
Larmor	$\vec{\tau} = \vec{\mu} \times \vec{B},\ \omega = -\gamma B$
Cap.	Depolarization of transmitted beam
App. St.	Observe depolarization effects of electromagnet as a function of position and current

I. Dhiman et al, *Rev. Sci. Instrum.* **88** 095103 (2017)

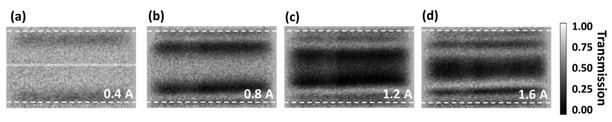

Polarized transmission neutron radiographs of a cylindrical coil with inner diameter = 19 mm, length = 150 mm, and 614 windings, measured as a function of current: (a) 0.4 A, (b) 0.8 A, (c) 1.2 A, (d) 1.6 A, using monochromatic neutron beam. Dotted lines in the radiographs indicate the coil diameter

Sc. A.	Materials & Engineering
Sc. Ex.	Single crystal of superconductor $YBa_2Cu_3O_7$
Cap. Fam.	Explore Magnetism
M-B	$(\boldsymbol{P} \cdot \boldsymbol{M}_\perp^\dagger)\boldsymbol{M}_\perp + (\boldsymbol{P} \cdot \boldsymbol{M}_\perp)\boldsymbol{M}_\perp^\dagger - \boldsymbol{P}(\boldsymbol{M}_\perp^\dagger \boldsymbol{M}_\perp)$
Cap.	Depolarization of transmitted beam
App. St.	Observe trapped fields within superconductor

T. Wang et al, *Rev. Sci. Instrum.* **90** 033705 (2019)

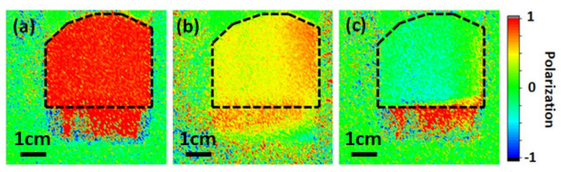

The sample area is labeled by a black dashed line: (a) zero trapped field, (b) FC trapped field of 7.5 G parallel to the YBCO block surface, and (c) FC trapped field of 15 G parallel to the YBCO block surface.

Sc. A.	Materials & Engineering
Sc. Ex.	Ferromagnetic powder Fe_3Pt
Cap. Fam.	Explore Magnetism
M-B	$(\boldsymbol{P} \cdot \boldsymbol{M}_\perp^\dagger)\boldsymbol{M}_\perp + (\boldsymbol{P} \cdot \boldsymbol{M}_\perp)\boldsymbol{M}_\perp^\dagger - \boldsymbol{P}(\boldsymbol{M}_\perp^\dagger \boldsymbol{M}_\perp)$
Cap.	Depolarization of transmitted beam
App. St.	Observe transition from ferromagnetic to paramagnetic state through T_c

I. Dhiman et al, *Rev. Sci. Instrum.* **88** 095103 (2017)

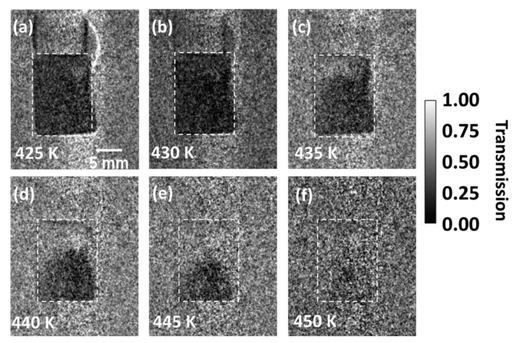

Polarized neutron radiographs for Fe3Pt (10 × 3 × 20 mm3) as a function of temperature, with an exposure time of 600 s: (a) 425 K, (b) 430 K, (c) 435 K, (d) 440 K, (e) 445 K, (f) 450 K. Measurements are carried out while heating the sample from 425 K to 450 K. White dashed boxes show the sample area. Contrast of the radiographs is enhanced artificially to improve the visualization of magnetic effects inside the sample.

Plans for more polarized imaging at both MARS & VENUS (SNS, BL-10)

Depolarization Imaging at J-PARC, RADEN (BL22)

Science Area	Materials & Engineering
Science Example	Inductor with Mn-Zn ferrite core
Capability Family	explore magnetic scattering
Larmor	$\vec{\tau} = \vec{\mu} \times \vec{B},\ \omega = -\gamma B$
Capability	Depolarization
Application Statement	Quantify field magnitude and direction within the ferrite core of an inductor, where direct probes cannot access

H. Mamiya *et al*, "Neutron imaging for magnetization inside an operating inductor," *Scientific Reports* **13**, 9184 (2023)

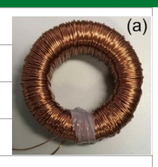

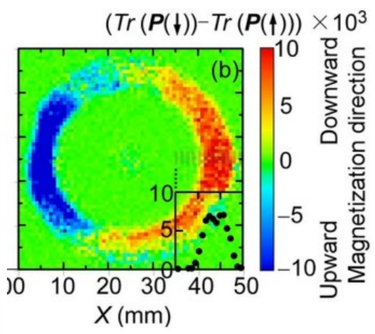

Depolarization Imaging at J-PARC, NOBORU (BL10)

Science Area	Materials & Engineering
Science Example	Electric motor
Capability Family	explore magnetic scattering
Larmor	$\vec{\tau} = \vec{\mu} \times \vec{B},\ \omega = -\gamma B$
Capability	Depolarization
Application Statement	Quantify field magnitude and direction within an electric motor, where direct probes cannot access

K. Hiroi *et al*, "Magnetic fieldimaging of amodel electric motor usingpolarizedpulsed neutrons at J-PARC/MLF," *Journal of Physics, Conference Series* **862**, 012008 (2017) (PNCMI)

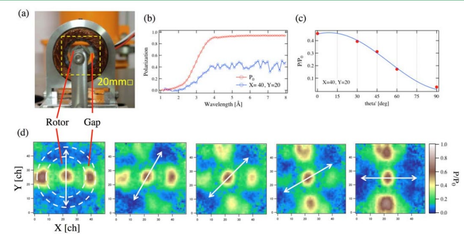

We're just getting started: Emerging polarized neutron configurations on fresh instruments

SHUG User meeting 2023
L. Debeer-Schmitt, H. Bilheux, Y. Zhang, M. Frontzek, C.Y. Jiang, L. Crow, F. Li

Polarized neutrons enable a variety of capabilities which enhance 'unpolarized' neutron scattering techniques by separating different aspects and dimensions of scattering, or providing high resolution in energy and/or angle. At ORNL, we are expanding the utility of polarized neutron scattering to more neutron scattering techniques, enabling a more nuanced understanding of the systems under study.

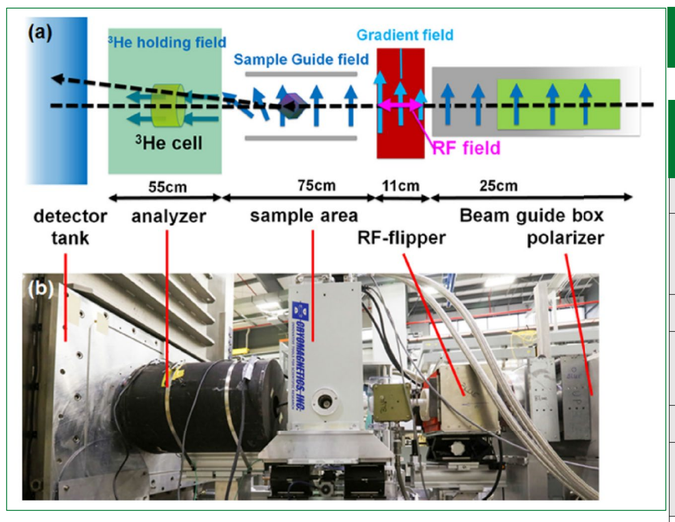

Small Angle Neutron Scattering at GP-SANS, HFIR CG-2

Longitudinal 1 Configuration (2 filters 1 flipper, spin-flip and non-spin-flip only)	
Science Area	Condensed matter
Science Example	Single crystal of helical magnet $Cr_{1/3}NbS_2$
Capability Family	Explore Magnetism
Relevant M-B terms	$(\boldsymbol{P}\cdot\boldsymbol{M}_\perp^\dagger)\boldsymbol{M}_\perp+(\boldsymbol{P}\cdot\boldsymbol{M}_\perp)\boldsymbol{M}_\perp^\dagger-\boldsymbol{P}(\boldsymbol{M}_\perp^\dagger\boldsymbol{M}_\perp)$
Capability	Compare M⊥ to M∥
Application Statement	Quantify ellipticity of chiral structure
T. Wang et al, *Physica B* **551** 492 (2018)	

Half Polarized Configuration (1 filter 1 flipper, intensity variations only)	
Sc. A.	Condensed matter
Sc. Ex.	Nanopillars of ferromagnetic $CoFe_2O_4$ in ferroelectric $BaTiO_3$
Cap. Fam.	Explore Magnetism
M-B	$\boldsymbol{P}\cdot\boldsymbol{M}_\perp^\dagger N+\boldsymbol{P}\cdot\boldsymbol{M}_\perp N^\dagger$
Cap.	Difference is predominantly a measure of M_z
App. St.	Compare to nano-pillar model to distinguish and locate 2 magnetic phases in nanopillars
T.O. Farmer et al, *Phys. Rev. Mat.* **3** 081401(R) (2019)	

Larmor Configuration (2 filter 2 Wollaston Prisms)	
Sc. A.	Materials & Engineering
Sc. Ex.	Mesoporous silica forming over time
Cap. Fam.	Enhance resolution
Larmor	$\vec{\tau}=\vec{\mu}\times\vec{B},\ \omega=-\gamma B$
Cap.	Up to 2.5 μm sensitivity via enhanced angle resolution
App. St.	Observe simultaneous emergence of large particles and Bragg peaks
J. Schmitt et al, *ACS Appl. Mater. Interfaces* **12** 28461 (2020) F. Li et al, *Sci Rep* **9** 8563 (2019)	

SEMSANS, ORNL prisms @ ISIS

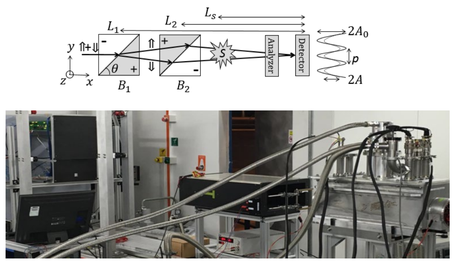

Upgrade planned for GP-SANS for more routine configuration changes

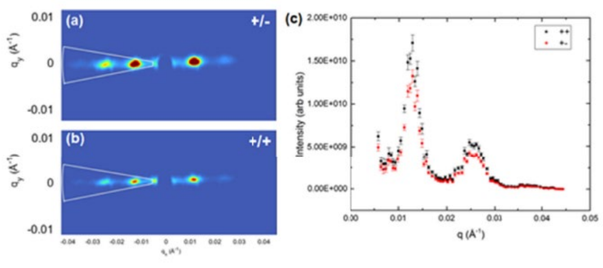

(a) Raw 2D scattering data of the +/- spin state of the helical magnets $Cr_{1/3}NbS_2$ (b) Raw 2D scattering data of the +/+ spin state of the helical magnets $Cr_{1/3}NbS_2$ (c) Peaks represent helical periodicity. Comparison between the two spin configurations of the azimuthal integrated scattering cross section as a function of Q after the effect of the ^{3}He decay has been taken into consideration

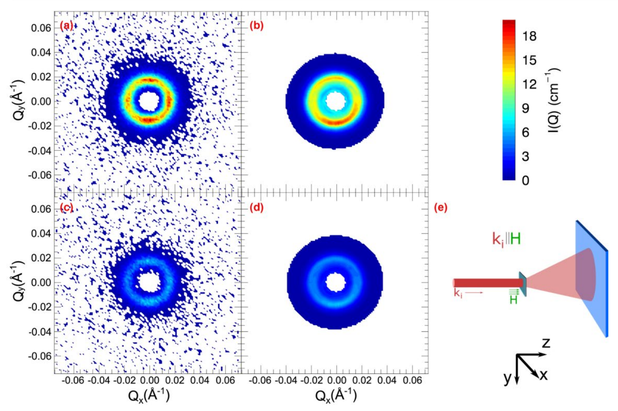

SANS with polarized neutron beam for +7 mT and model fit: (a),(b) I+(Q), (c),(d) I−(Q). The ring feature is identified at Q = 0.0168 Å^{-1}. (e) Schematic of neutron experiment. The final wave vector $\mathbf{k_f}$ lies inside the cone. The scattering vector **Q** lies in the green colored plane at the position of the sample. Pillars parallel to the incident beam and the neutron beam polarization. Samples were saturated with a +7 T out-of-plane field ex situ and then measured at +7 mT (near remanence) and −500 mT field where the sign is taken with respect to the saturation field

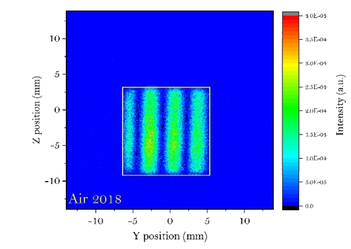

Intensity modulation of one of the spin states with air being the blank. The wavelength of this frame is 6.27Å. The the yellow box indicates the area of interest used to calculate Γ

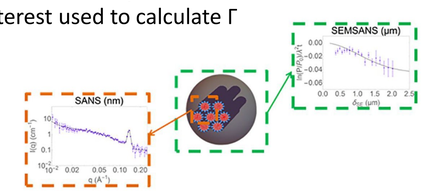

Longitudinal 1 Configuration (2 filters, 0 flipper, non-spin-flip only) Depolarization Imaging at MARS, HFIR CG-1D

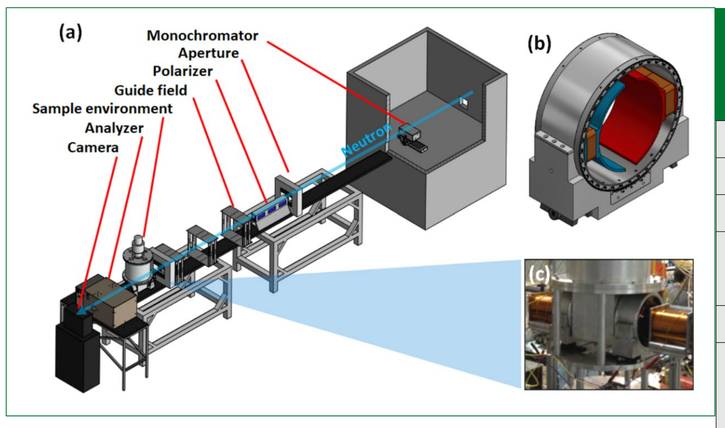

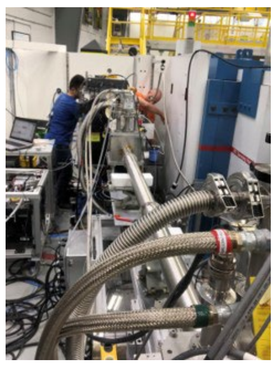

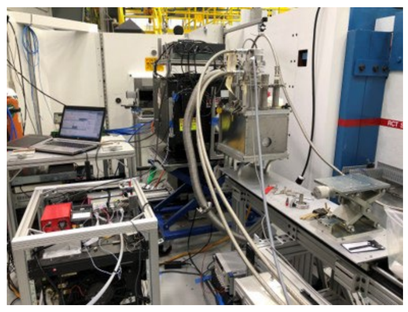

Longitudinal 1 Configuration (2 filters, 0 flipper, non-spin-flip only) Depolarization Imaging at MARS, HFIR CG-1D	
Sc. A.	Condensed matter
Sc. Ex.	Cylindrical coil at varying current
Cap. Fam.	Explore Magnetism
Larmor	$\vec{\tau}=\vec{\mu}\times\vec{B},\ \omega=-\gamma B$
Cap.	Depolarization of transmitted beam
App. St.	Observe depolarization effects of electromagnet as a function of position and current
I. Dhiman et al, *Rev. Sci. Instrum.* **88** 095103 (2017)	

Sc. A.	Condensed matter
Sc. Ex.	Single crystal of superconductor $YBa_2Cu_3O_7$
Cap. Fam.	Explore Magnetism
M-B	$(\boldsymbol{P}\cdot\boldsymbol{M}_\perp^\dagger)\boldsymbol{M}_\perp+(\boldsymbol{P}\cdot\boldsymbol{M}_\perp)\boldsymbol{M}_\perp^\dagger-\boldsymbol{P}(\boldsymbol{M}_\perp^\dagger\boldsymbol{M}_\perp)$
Cap.	Depolarization of transmitted beam
App. St.	Observe trapped fields within superconductor
T. Wang et al, *Rev. Sci. Instrum.* **90** 033705 (2019)	

Sc. A.	Condensed matter
Sc. Ex.	Ferromagnetic powder Fe_3Pt
Cap. Fam.	Explore Magnetism
M-B	$(\boldsymbol{P}\cdot\boldsymbol{M}_\perp^\dagger)\boldsymbol{M}_\perp+(\boldsymbol{P}\cdot\boldsymbol{M}_\perp)\boldsymbol{M}_\perp^\dagger-\boldsymbol{P}(\boldsymbol{M}_\perp^\dagger\boldsymbol{M}_\perp)$
Cap.	Depolarization of transmitted beam
App. St.	Observe transition from ferromagnetic to paramagnetic state through T_c
I. Dhiman et al, *Rev. Sci. Instrum.* **88** 095103 (2017)	

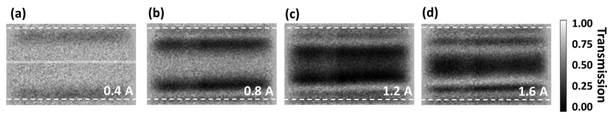

Polarized transmission neutron radiographs of a cylindrical coil with inner diameter = 19 mm, length = 150 mm, and 614 windings, measured as a function of current: (a) 0.4 A, (b) 0.8 A, (c) 1.2 A, (d) 1.6 A, using monochromatic neutron beam. Dotted lines in the radiographs indicate the coil diameter

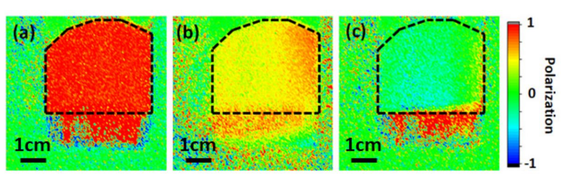

The sample area is labeled by a black dashed line: (a) zero trapped field, (b) FC trapped field of 7.5 G parallel to the YBCO block surface, and (c) FC trapped field of 15 G parallel to the YBCO block surface.

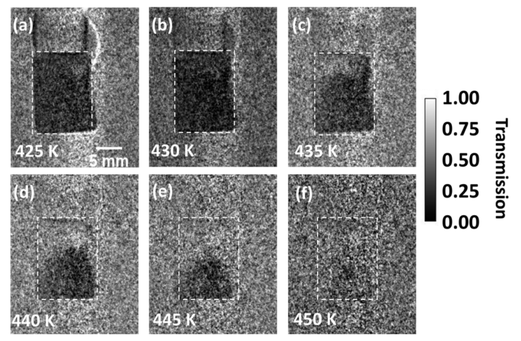

Polarized neutron radiographs for Fe3Pt (10 × 3 × 20 mm3) as a function of temperature, with an exposure time of 600 s: (a) 425 K, (b) 430 K, (c) 435 K, (d) 440 K, (e) 445 K, (f) 450 K. Measurements are carried out while heating the sample from 425 K to 450 K. White dashed boxes show the sample area. Contrast of the radiographs is enhanced artificially to improve the visualization of magnetic effects inside the sample.

Plans for more polarized imaging at both MARS & VENUS (SNS, BL-10)

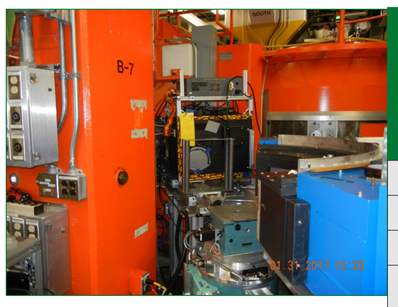

Half-Polarized Configuration
(1 filter, 1 flipper, changes in scattered intensity only)
Powder Diffraction at WAND², HFIR HB-2C

Science Area	Condensed matter
Science Example	Polycrystalline ferromagnet Fe
Capability Family	Explore Magnetism
Relevant M-B terms	$\boldsymbol{P}\cdot\boldsymbol{M}_\perp^\dagger N+\boldsymbol{P}\cdot\boldsymbol{M}_\perp N^\dagger$
Capability	Determine magnetization density
Application Statement	Initial demonstration, magnetization density in room temperature Fe rod
unpublished; early demonstration	

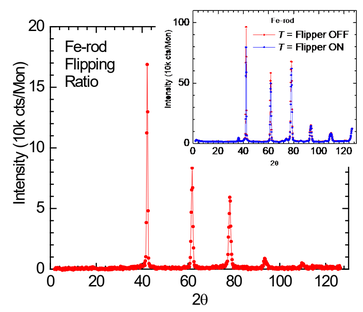

Configurations to enhance contrast access either changes in scattered neutron **intensity** and/or **polarization state**.
Capabilities access specific contributions to these changes, either as found in the Maleev-Blume equations, via Larmor precession of the neutrons, or via changes in absorption.
***Configurations* to enhance resolution leverage Larmor precession before and/or after the sample.**

Instruments with Polarization Configurations at HFIR & SNS

Polarization Steering Committee

Half-Polarized, Longitudinal-1, Spherical Neutron Polarimetry & Larmor/Wollaston Configurations Diffraction & Spectroscopy

Limited Polarization Development

We're just getting started

Half-Polarized Configuration Powder Diffraction

We're just getting started

Half-Polarized Dynamic Nuclear Polarization Configuration Single Crystal Diffraction

Half-Polarized Configuration Single Crystal Diffraction

Trying out exciting new polarization configurations and capabilities

HFIR Beryllium Reflector Replacement Project

Half-Polarized, Longitudinal-1, Spherical Neutron Polarimetry & Larmor/Wollaston Configurations Diffraction & Spectroscopy

From demonstration to user program

Losing a critical polarization development station

Larmor Configuration, Spectroscopy

Half-Polarized Dynamic Nuclear Polarization Configuration Single Crystal Diffraction, *ALL PISTONS FIRING*

Half-Polarized, Longitudinal-1, & Longitudinal-2 Configurations Reflectometry

Larmor Configuration, Spectroscopy

Half-Polarized & Longitudinal-1 Configurations Diffraction & Spectroscopy

Leverages Polarized Neutrons for some long-term experiments

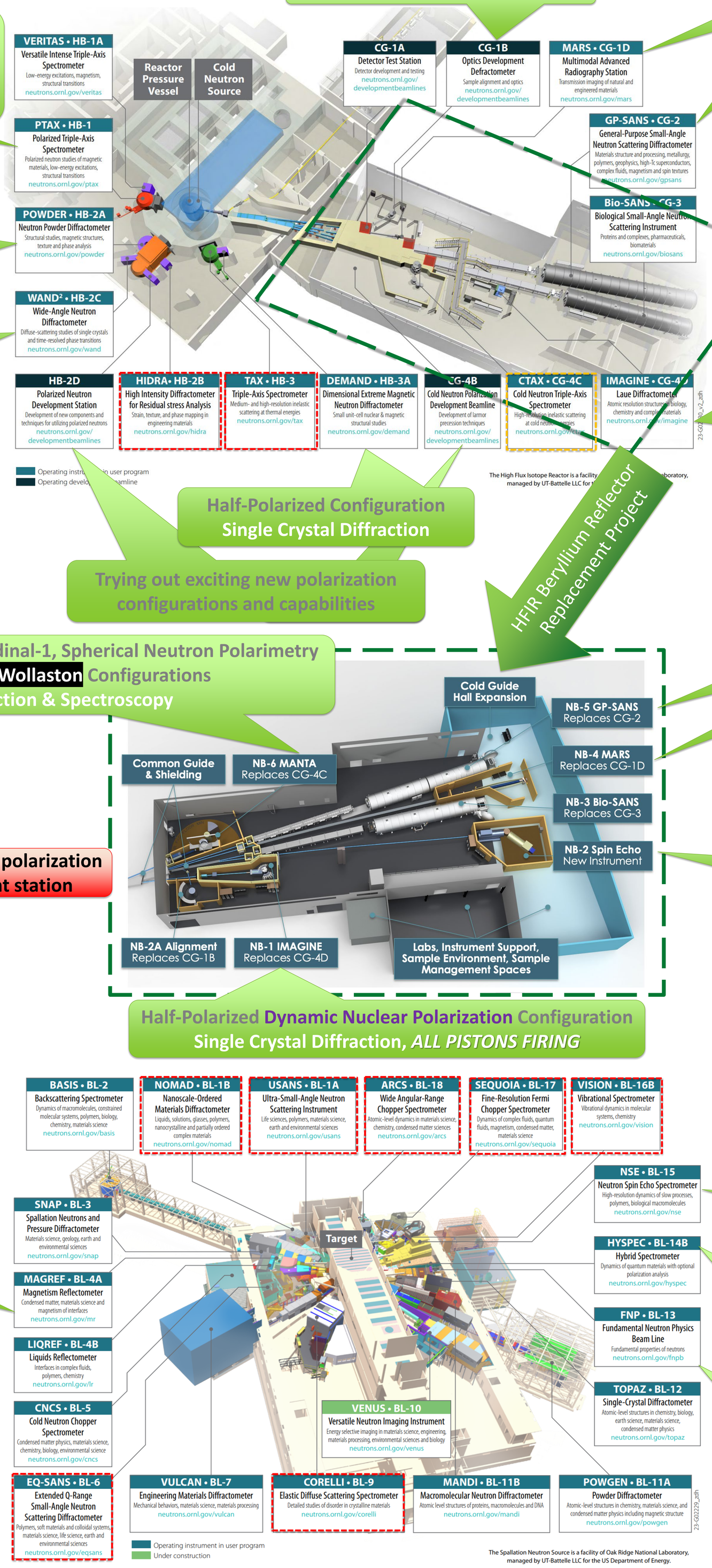

Those few instruments which will never utilize polarized neutrons…

OAK RIDGE National Laboratory | HIGH FLUX ISOTOPE REACTOR | SPALLATION NEUTRON SOURCE

Research was performed at HFIR and SNS, DOE Office of Science User Facilities

Oak Ridge National Laboratory is managed by UT-Battelle LLC for the US Department of Energy

U.S. DEPARTMENT OF ENERGY | Office of Science

Polarized Neutrons & X-Ray Dichroism: Complementary Diagnostics for Magnetism

25th National School on Neutron & X-Ray Scattering, 2023

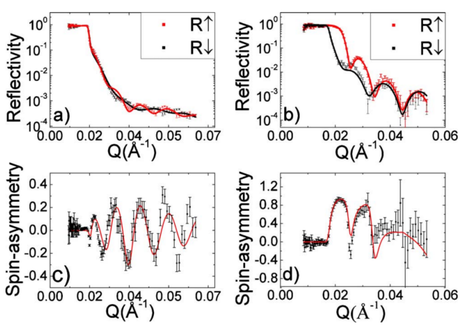

FIG. 3. (Color online) Polarized neutron reflectivity recorded with an applied field of $\mu_0 H$=0.34 T at (a) 300 K and (b) 400 K. (c) and (d) are the spin asymmetry at 300 K and 400 K, respectively.

Polarized Neutrons	X-ray Dichroism
ISIS	NSLS (1)
CRISP	U4B
<configuration>	<configuration>
Condensed matter physics	
FeRh epilayers near the ferromagnetic / antiferromagnetic transition temperature	
Reflectometry	
<capability>	<capability>
<capability family>	<capability family>
R. Fan *et al*, "Ferromagnetism at the interfaces of antiferromagnetic FeRh epilayers", *Phys. Rev. B* **82**, 184418 (2010)	
Y. Ding *et al*, "Bulk and near-surface magnetic properties of FeRh thin films", *J. Appl. Phys.* **103**, 07B515 (2008)	

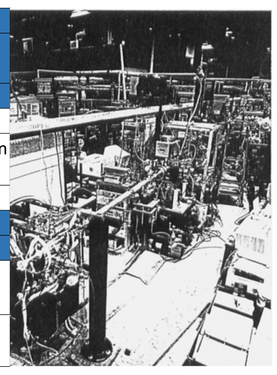

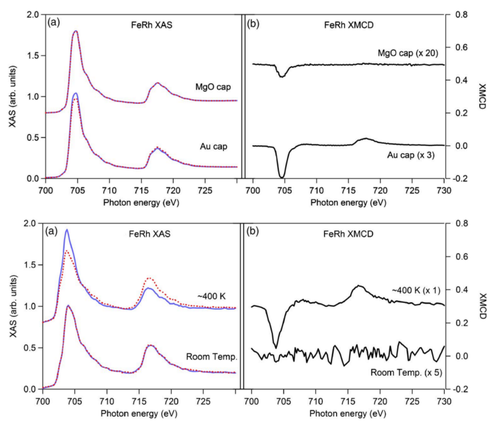

FIG. 2. (Color online) Room-temperature, TEY mode XAS spectra of 500 Å $Fe_{48}Rh_{52}$ thin films on MgO (001) capped with either 20 Å of Au or MgO. (b) XMCD spectra for the same films. Note the scale factors.

FIG. 3. (Color online) Ambient and elevated temperature XAS spectra of a 500 Å $Fe_{48}Rh_{52}$ thin film on MgO (001) capped with 20 Å of Au. (b) Corresponding XMCD spectra. Again, note the scale factors.

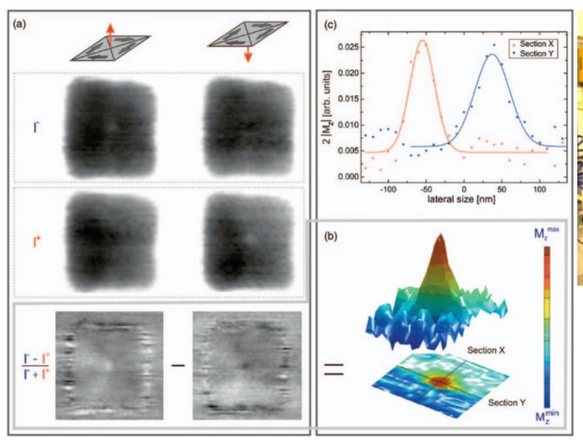

FIG. 2. (Color) Panel (a) shows the static configuration of a vortex structure (sample A: 500×500 nm², 40 nm thick) with a vortex core pointing up (left column) and down (right column). In the first row, images were taken for negative polarization of the photons (I^-) while images with opposite polarization (I^+) are shown in the second row. The "dichroic image" is depicted in the third row. A white or black spot can be observed, corresponding to a vortex core pointing up or down, respectively. The two dichroic images were subtracted from one another and a 3D image is given in panel (b) (200×200 nm² cut). The distributions along sections X and Y are plotted in panel (c) with the corresponding Gaussian fits in order to estimate the size of the vortex core.

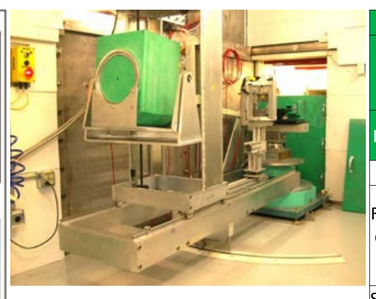

Polarized Neutrons	X-ray Dichroism
Lujan Neutron Scattering Center	Advanced Light Source
Asterix spectrometer in GI-SANS mode	Scanning Transmission X-ray Microscope (STXM) beamline
Half Polarized and Longitudinal 1	X-Ray circular dichroism
Condensed matter	
Fe dots with transition from single domain to ***vortex*** as a function of dot diameter and magnetic field	$Ni_{80}Fe_{20}$ permalloy thin film (40 nm) with single magnetic ***vortex***
Small Angle Neutron Scattering	Soft X-ray Microscopy
Depth profile	Transverse profile
I.V. Roshchin *et al*, 'Measurement of the vortex core in sub-100nm Fe dots using polarized neutron scattering,' *EPL* **86** 67008 (2009)	
K.W. Chou *et al*, 'Direct Observation of the vortex core magnetizationand its dynamics,' *App. Phys. Lett.* **90**, 202505 (2007)	

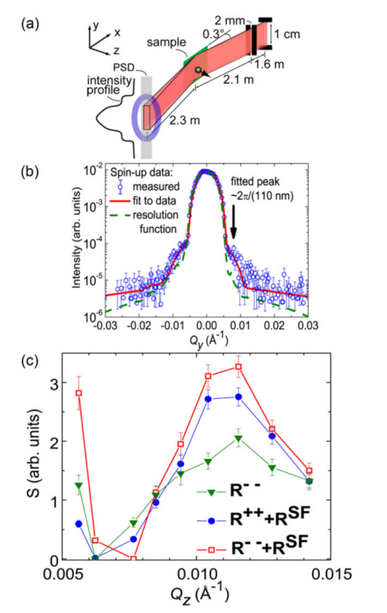

Fig. 3: (Colour on-line) (a) Schematic of the experimental setup. (b) Polarized neutron scattering as a function of scattering vector component Q_y for $Q_z = 0.011$ Å^{-1}. (c) Integrated neutron scattering intensity from the dots as a function of Q_z.

Polarized Neutrons	X-ray Dichroism
NIST Center for Neutron Scattering	Advanced Photon Source
NG1 reflectometer	4ID-D
Longitudinal 2	Circular Dichroism
Condensed matter	
Fe & Gd multilayer	
Reflectometry	
E. Kravtsov *et al*, 'Complementary polarized neutron and resonant x-ray magnetic reflectometry measurements in Fe/Gd heterostructures: Case of inhomogeneous interalayer magnetic structure,' *Phys. Rev. B* **79** 134438 (2009)	

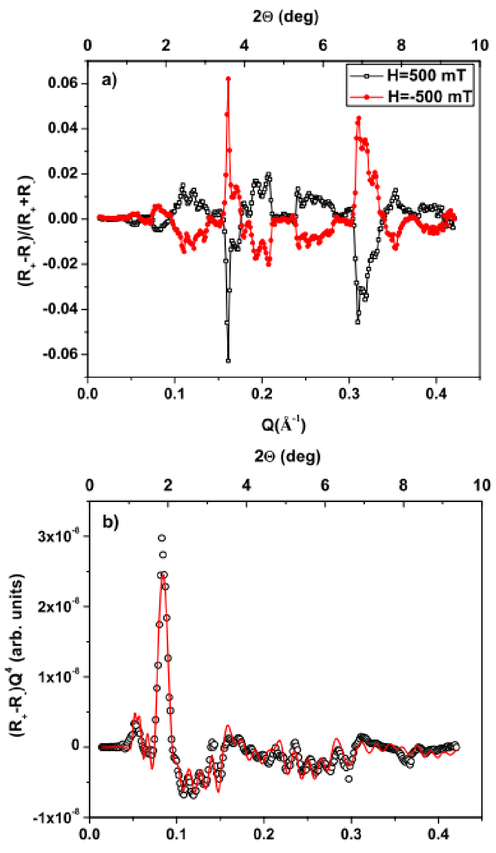

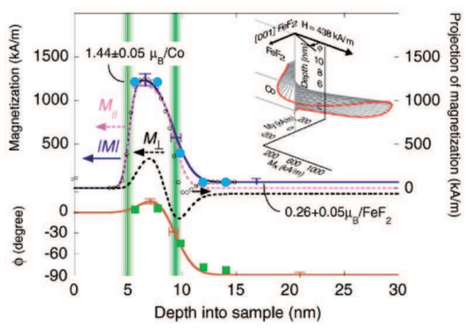

Figure 4. Depth dependence of the vector magnetization (inset, 3D view), magnitude (blue curve, $|M|$), and angular deviation ϕ (red curve) from the applied field in the sample plane deduced from neutron scattering. Error bars represent deviations of depth profiles with indistinguishable χ^2. The magnetization used in the OOMMF simulation is indicated by • and the values of ϕ are indicated by ■ obtained from the simulation. The sum of the Fe and Co spin density profiles of $H\|[0\,0\,1]FeF_2$ (obtained from figure 2 in arbitrary units using X-ray scattering) is shown in absolute units (○).

Polarized Neutrons	X-ray Dichroism
Lujan Neutron Scattering Center	Advanced Light Source
Reflectometer	Reflectometer
Longitudinal 2	circular dichroism
Condensed matter	
single crystal of antiferromagnetic FeF_2 capped with a ferromagnetic Co film	
Specular reflectivity & off-specular scattering	
spatial distribution of different vector components of the magnetization	magnetization with element-selectivity
S.K. Sinha *et al*, 'Combined neutron and synchrotron studies of magnetic films,' *Pramana-J. Phys.* **67** 47-55 (2006)	

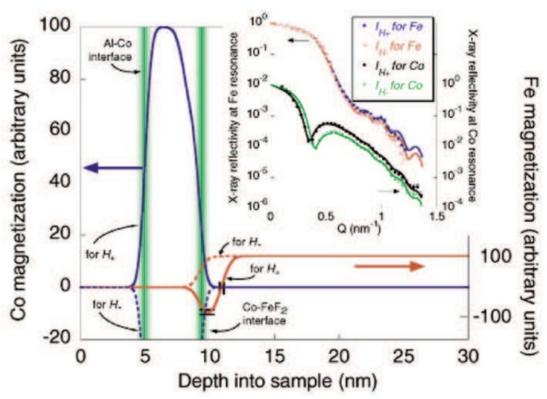

Figure 3. Spin density depth profiles for Co (blue) and Fe (red) spins obtained from the specular X-ray reflectivities (inset) at $H_\pm = \pm 796$ kA/m.

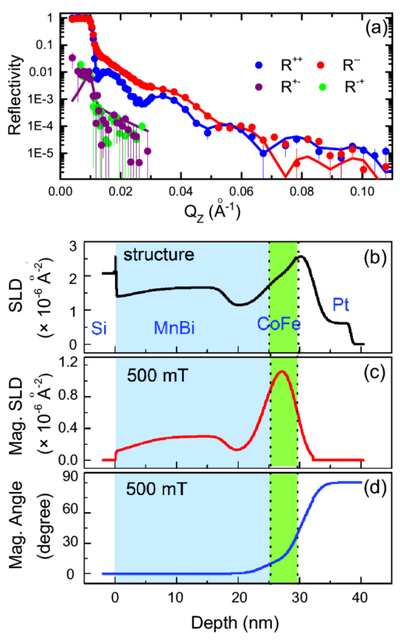

Figure 2. Polarized neutron reflectivity measurements. (a) experimental results and corresponding fits (solid lines) for all four cross sections, R++ (blue), R+- (purple), R-+ (green) and R-- (red) obtained in a field of 0.5 T applied parallel to the sample plane of a MnBi(25 nm)/$Co_{70}Fe_{30}$(5 nm) bilayer after saturation in a perpendicular field of 1.6 T (Note: error bars displayed here indicate 1 standard deviation); and (b)-(d) depth profiles of a MnBi(25 nm)/$Co_{70}Fe_{30}$(5 nm) bilayer: (b) structural scattering length density (SLD), (c) magnetic scattering length density which is proportional to the in-plane component of the magnetization, and (d) angle of the in-plane magnetization component relative to the 0.5 T in-plane field at 0° obtained from fits to polarized neutron reflectometry measurements. The rotation of the in-plane magnetization as a function of depth from 0° near the MnBi/Co-Fe interface to 90° near the Co-Fe/Pt interface is consistent with presence of the curling mode.

Polarized Neutrons	X-ray Dichroism
NIST Center for Neutron Research	Advanced Light Source
PBR & MAGIK reflectometers	???
Longitudinal 2	circular dichroism
Condensed matter	
exchange-coupled MnBi:Co-Fe (hard:soft) magnetic bilayers	
Reflectometry	
X.H. Zhang *et al*, 'Interfacial magnetic vortex formation in exchnage-coupled hard-soft magnetic bilayers,' *J. of Magnetism and Mag. Materials* **560** 169627 (2022)	

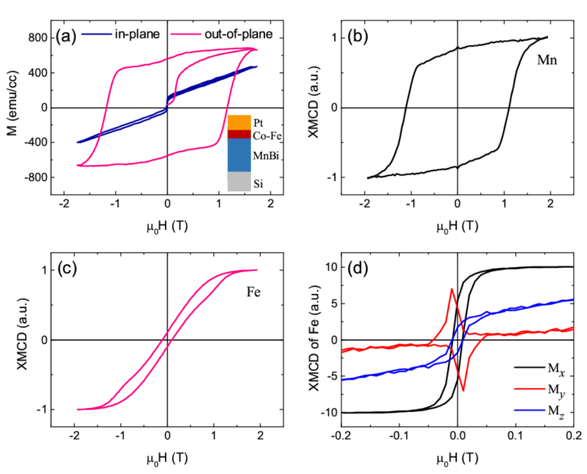

Figure 1. Hysteresis loops of a MnBi(20 nm)/$Co_{70}Fe_{30}$(3 nm) bilayer sample. (a) the in-plane and out-of-plane hysteresis loops obtained by VSM; and element-sensitive room-temperature XMCD hysteresis loops: (b) out-of-plane loop for Mn, (c) out-of-plane loop for Fe, and (d) in-plane loops for Fe with M_x (black), M_y (red) and M_z (blue) components. Note that the scale of M_y and M_z is magnified by a factor of 10.

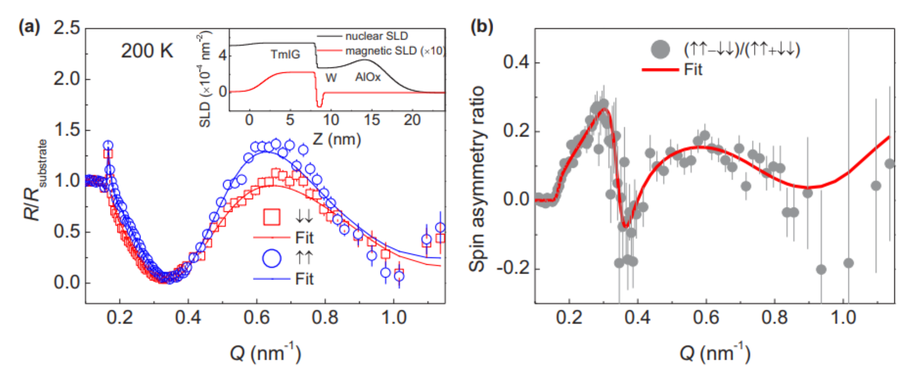

FIG. 4. Capturing the spin textures in the W(5 nm)/TmIG(10 nm) by neutron techniques at 200 K. (a) Polarized neutron reflectivities (with a 700-mT in-plane field) for the spin-polarized $R^{\uparrow\uparrow}$ and $R^{\downarrow\downarrow}$ channels. Inset: Corresponding models with structural and magnetic scattering length densities (SLDs) used to obtain the best fits. (b) The spin asymmetry ratio $(R^{\uparrow\uparrow} - R^{\downarrow\downarrow})/(R^{\uparrow\uparrow} + R^{\downarrow\downarrow})$ between the $R^{\uparrow\uparrow}$ and $R^{\downarrow\downarrow}$ channels. The error bars are ±1 s.d.

Polarized Neutrons	X-ray Dichroism
NIST Center for Neutron Research	Advanced Light source
PBR	???
Longitudinal 2	Circular Dichroism
Condensed matter physics	
Multilayer with ferrimagnetic insulator and heavy metal layers which exhibits an anamalous Hall effect	
reflectometry	
Q. Shao *et al*, 'Exploring interfacial exchange coupling and sublattice effect in heavy metal/ferrimagnetic insulator heterostructures using Hall measurements, x-ray magnetic circular dichroism, and neutron reflectometry,' *Phys. Rev. B* **99** 10441 (2019)	

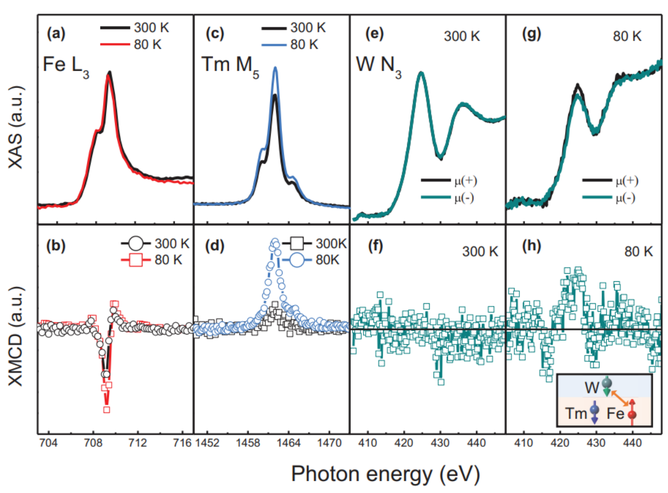

FIG. 3. Capturing the exchange interactions in the W(5 nm)/TmIG(10 nm) by x-ray techniques. (a) XAS and (b) XMCD spectra taken at the Fe L_3 edge at 80 and 300 K. (c) XAS and (d) XMCD spectra taken on the Tm M_5 edge at 80 and 300 K. XAS taken on the W N_3 edge at 300 K (e) and 80 K (g) with two opposite x-ray helicities, $\mu(+)$ and $\mu(-)$. XMCD at the W N_3 edge taken at 300 K (f) and 80 K (h). The inset in (h) illustrates relative spin alignments of the Fe, Tm, and induced W moment at 80 K based on the sign of XMCD.

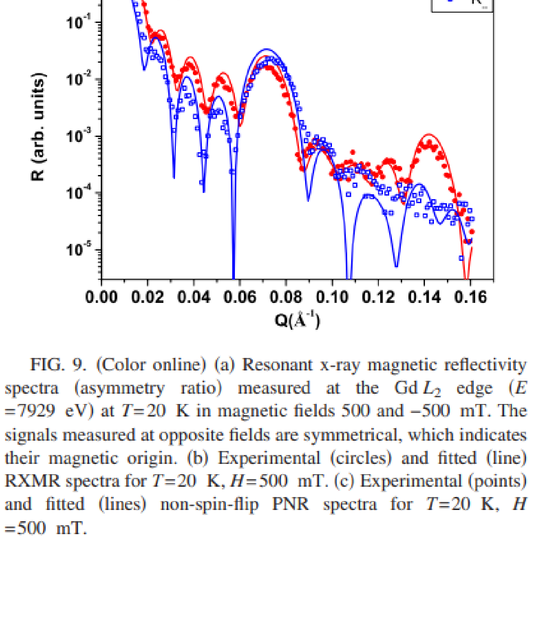

FIG. 9. (Color online) (a) Resonant x-ray magnetic reflectivity spectra (asymmetry ratio) measured at the Gd L_2 edge (E =7929 eV) at T=20 K in magnetic fields 500 and −500 mT. The signals measured at opposite fields are symmetrical, which indicates their magnetic origin. (b) Experimental (circles) and fitted (line) RXMR spectra for T=20 K, H=500 mT. (c) Experimental (points) and fitted (lines) non-spin-flip PNR spectra for T=20 K, H =500 mT.